Magnetic and thermodynamic properties of cobalt-doped iron pyrite: Griffiths phase in a magnetic semiconductor

S. Guo,[1] D. P. Young,[1] R. T. Macaluso,[2] D. A. Browne,[1] N. L. Henderson,[1] J. Y. Chan,[2] L. L. Henry,[3] and J. F. DiTusa[1]
[1]*Department of Physics and Astronomy, Louisiana State University, Baton Rouge, Louisiana 70803, USA*
[2]*Department of Chemistry, Louisiana State University, Baton Rouge, Louisiana 70803, USA*
[3]*Department of Physics, Southern University, Baton Rouge, Louisiana 70813, USA*
(Received 14 December 2009; revised manuscript received 25 February 2010; published 26 April 2010)

Doping of the band insulator FeS_2 with Co on the Fe site introduces a small density of itinerant carriers and magnetic moments. The lattice constant, ac and dc magnetic susceptibility, magnetization, and specific heat have been measured over the $0 \leq x \leq 0.085$ range of Co concentration. The variation in the ac susceptibility with hydrostatic pressure has also been measured in a small number of our samples. All of these quantities show systematic variation with x including a paramagnetic to disordered ferromagnetic transition at $x = 0.007 \pm 0.002$. A detailed analysis of the changes with temperature and magnetic field reveal small power-law dependencies at low temperatures for samples near the critical concentration for magnetism and just above the Curie temperature at higher x. In addition, the magnetic susceptibility and specific heat are nonanalytic around $H=0$ displaying extraordinarily sharp field dependence in this same temperature range. We interpret this behavior as due to the formation of Griffiths phases that result from the quenched disorder inherent in a doped semiconductor.

DOI: 10.1103/PhysRevB.81.144423 PACS number(s): 75.50.Pp, 75.40.−s, 75.20.Hr

I. INTRODUCTION AND MOTIVATION

The desire for ever increasing computational speeds has led to the conception of spintronics technologies that make use of both the charge and spin properties of electrical charge carriers in solids.[1,2] Realization of these devices for useful technologies requires the discovery and development of materials that have easily controllable electronic and magnetic properties to the same extent that semiconductors allow control over charge properties. This demand has led to an enormous interest in magnetic semiconductors to investigate if traditional semiconductors can be manipulated by chemical substitution of transition metal elements, or other creative means, into offering control over the spin properties of electrons.[3–8] Because so many of the suggested devices rely on the production and detection of spin polarized currents, magnetic semiconductors with Curie temperatures above room temperature that are compatible with silicon technology are highly desired. However, this goal has thus far not been met and it has become increasingly apparent that to make progress, fundamental knowledge and understanding of the electronic and magnetic properties of magnetic semiconductors are necessary. Although some headway in this direction has been made, the complexity of disordered materials with strong interactions makes magnetic semiconductors difficult to model and understand.[9–11]

In a recent paper, we presented the results of an exploration into the magnetic and electronic properties of one such magnetic semiconducting compound, $Fe_{1-x}Co_xS_2$ based on the diamagnetic insulating parent compound iron pyrite (FeS_2).[12] We found that the insulator-to-metal transition that occurs for low concentrations of Co doping was followed by a transition from a paramagnet to a disordered ferromagnet first apparent for small dopant concentrations, x, at very low temperatures. Increased Co doping led to an increased transition temperature and to a more ordered ferromagnetic phase.[13–17] The main conclusion of our paper was that the quenched disorder associated with the chemical substitution has important consequences on the formation of the magnetic state at small x and on the finite-temperature phase transitions at larger x. Unusual power-law temperature, T, and magnetic field, H, dependencies of the magnetic susceptibility, magnetization, and specific heat were measured at low T for x near the critical concentration for nucleation of a magnetic phase, x_c, as well as at T's just above the Curie temperature, T_c for $x > x_c$. These were attributed to large, rare disorder fluctuations consisting of regions of local magnetic order which fluctuate as a single large magnetic moment and that grow in size as $T \to 0$ or $T \to T_c$. Fluctuating rare region phenomena associated with phase transitions in systems with quenched disorder are known under the heading of Griffiths phases.[18–20]

Theorists have found the subject of Griffiths phases fascinating since Griffiths discovered the nonintuitive feature in his calculations that, under certain conditions, exponentially rare regions in disordered systems can dominate the thermodynamic response when in proximity to a phase transition.[18,20] This is in contrast to many aspects of phase transitions where disorder can be treated perturbatively or simply ignored. These ideas have drawn even more interest as evidence for non-Fermi liquid behavior in disordered systems has been discovered while explanations remain tentative.[21] While it is clear that the disorder and strong electron correlations are responsible for the breakdown of Fermi liquid behavior in some cases, the microscopic origins remain poorly understood.[19] In this context, the unusual power-law behavior associated with the formation of Griffiths phases have been discussed as one mechanism for disorder driven non-Fermi liquid behavior.[22,23] Experimental evidence that Griffiths phases are observable in condensed matter systems has only recently been reported for a small number of systems[24–28] and in our previous publication we

presented evidence for the importance of Griffiths phase formation near the critical concentration for magnetic ordering in the magnetic semiconducting system $Fe_{1-x}Co_xS_2$. The purpose of the present paper is to present a more thorough rendering of our magnetic susceptibility, magnetization, and specific heat experiments and analysis, as well as to present the results of some more recent ac magnetic susceptibility measurements made at ambient and applied pressures of up to 7 kbar. In a separate accompanying article we present the results of our Hall effect and resistivity measurements of these same materials.[29]

We chose to investigate Co doped FeS_2 since FeS_2 is a simple diamagnetic band insulator with the same pyrite crystal structure as CoS_2, a itinerant ferromagnet.[13,14,30] The two compounds had been shown earlier to be miscible such as to form the substitutional series $Fe_{1-x}Co_xS_2$ without observation of second phases or any phase segregation that occurs in many magnetic semiconducting compounds. As such, it allowed the investigation of the transition from diamagnetic insulator to a paramagnetic metal, then to a ferromagnetic metal with Co substitution. In addition, band structure calculations have predicted that at large x, $0.5 \leq x \leq 0.95$, $Fe_{1-x}Co_xS_2$ is half metallic having a fully spin polarized ground state.[15–17,31]

We begin our discussion by presenting the details of the experimental techniques that we have used to investigate the extrinsic properties of $Fe_{1-x}Co_xS_2$. This is followed by a presentation of the magnetic susceptibility, magnetization, and specific heat over a wide range of x covering insulating, paramagnetic metallic, and ferromagnetic metallic behaviors. In Sec. IV we explore in detail the behavior of our crystals nearest x_c at low temperatures where the power law in T and H behaviors are found. This is followed by a discussion of the magnetic properties of crystals with $x > x_c$ in proximity to T_c displaying similar behavior. We conclude the paper with a summary and discussion of our results.

II. EXPERIMENTAL DETAILS

Single crystals of $Fe_{1-x}Co_xS_2$ were synthesized from high purity starting materials, including Fe powder (Alfa Aesar 99.998%), Co powder (Alfa Aesar 99.998%), and sulfur (Alfa Aesar 99.999%). These materials were sealed in a 16 mm diameter quartz tube under vacuum. Iodine (Alfa Aesar 99.99+%) was added to the tube as the transport agent at a concentration level of 2 to 5 gm/cm^3. The tubes were then placed in a small, single zone horizontal tube furnace (Lindberg/Blue Model 55035) and heated to a constant temperature. Insulating plugs were removed from the ends of the furnace to create a natural temperature gradient of ~50 °C. The charge was placed at the center of the furnace (hot zone), and single crystals would begin to form at the cold end of the tube in approximately five days, with a maximum yield by no later than 14 days. Good crystals were produced for temperatures in the range of 650 to 850 °C. Crystals were etched in HCl to remove any remaining flux.

Initial characterization included single crystal x-ray diffraction. Single crystal fragments were glued to a glass fiber and mounted on the goniometer of a Nonius Kappa charge coupled device diffractometer equipped with Mo-K_α radiation (wavelength=0.71073 Å). All x-ray structure determinations are consistent with a Pyrite crystal structure with no anomalous intensities that could be interpreted as evidence for a second phase. The model of the structure was refined to a level consistent with a fully solved crystal structure. We observe no evidence for disorder, including that associated with sulfur deficiencies or iodine inclusions, in the crystal structure of all our crystals. The lattice constants, a, shown in Fig. 1 were determined by the x-ray diffraction measurements. As displayed in the figure, a increases systematically with Co concentration, x in $Fe_{1-x}Co_xS_2$, beyond the lattice constant for pure FeS_2, $a=0.54165$ nm, and is comparable to the measurements of Refs. 14–17. The increase in lattice constant with x is consistent with Vegard's law and the idea that Co replaces Fe within the pyrite crystal structure. Energy-dispersive x-ray (EDX) microanalysis on a JEOL scanning electron microscope equipped with a Kevex Si(Li) detector was performed to check the stoichiometry of our samples. These revealed that the Co concentration was about 0.7 ± 0.1 times the nominal Co concentration of the starting materials, while the sum of the Co and Fe densities was within error, ±2%, of one half the sulfur density. The density of iodine in our samples was determined by this method to be 20 ppm on average and no sample was found to have an iodine concentration of higher than 100 ppm.

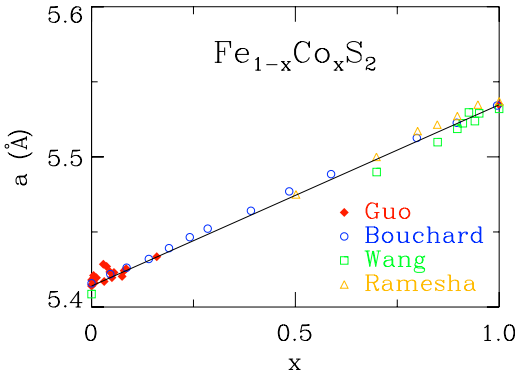

FIG. 1. (Color online) Lattice constants. Lattice constant, a, for a wide range of cobalt concentration, x, determined by single crystal x-ray diffraction for our samples (labeled Guo) along with comparisons with those previously determined. (Refs. 14–17) Black line is a linear x dependence of a from FeS_2 through to CoS_2.

Magnetization, M, and magnetic susceptibility (both ac and dc) measurements were performed in a Quantum Design superconducting quantum interference device (SQUID) magnetometer for temperatures, $T \geq 1.8$ K and dc magnetic fields, H, of up to 5 T. ac susceptibility measurements were carried out over a range of excitation fields from 0.1 to 1.5 Oe and excitation frequencies from 1 Hz to 1 kHz. In addition, ac magnetic susceptibility measurements were performed in a dilution refrigerator above 50 mK at $H=0$, a frequency of 1 kHz, and an excitation field of 1.5 Oe. Since our magnetization and susceptibility measurements were performed inside of a superconducting solenoid, particular care was employed to determine the zero of magnetic field for our low field measurements. This included oscillating the current in the magnet windings through zero several times with de-

caying amplitude, followed by measurements of $M(H)$ with 0.5 Oe steps to determine the minimum absolute value of the magnetization signal. In this manner we were able to identify $H=0$ to within 1 Oe. This procedure was of particular importance for our measurements of the low field ac susceptibility for samples with $x \leq 10x_c$ where the susceptibility was highly field dependent.

The saturation magnetization was determined by dc magnetization measurements at 1.8 K and high fields (up to 5 T). These measurements were consistent with our EDX measurements showing a magnetic moment density of 0.7 ± 0.1 times the nominal Co concentration. Because M measurements are easily performed and highly reproducible, we have subsequently used the saturated magnetization to determine the Co concentration of our samples. Thus, throughout this manuscript the stoichiometry of the samples noted in the figures and text was determined in this manner. The variations in the saturated magnetization for crystals from the same growth batch were measured to be $\pm 10\%$ of the average value. Therefore, we report x determined from measurements of M at high field for the crystals used in each of our measurements. Because the EDX and the high field $M(H)$ determinations of x scale well with the nominal Co concentrations for a large number of samples, we are confident that we have not imposed any implicit correlations on the data. Wherever possible, the same crystal was employed for several different measurement types, particularly for the measurement of the ac susceptibility and specific heat below 1 K.

The magnetic susceptibility of several of our crystals was measured with applied pressure ranging from ambient to 7 kbar in a beryllium-copper pressure cell.[32] Our pressure cell was based on previously published designs.[33–35] The pressure cell was machined from beryllium-copper alloy 25 since this material has a low magnetic susceptibility and superior mechanical properties. After machining, the cell was annealed in air at a temperature of 335 °C for 2 h. We designed our pressure cell to have a length of 12 cm to reduce the background seen by the SQUID pickup coils originating from the ends of the cell. The pistons are made from high purity Technox 3000 zirconia rods from Dynamic Ceramic. This resulted in a small, diamagnetic, ($\sim -7 \times 10^{-6}$ emu at 50 Oe field) background signal due to the lack of zirconia at the sample position. This background depended slightly on the distance between the ends of the two zirconia rods which, in turn, depended on the sample thickness, increasing for larger separations. The sample was placed inside a Teflon container which was sealed with a beryllium-copper cap and retainer. The Teflon container is filled with silicon oil (Dow Corning 704) as the pressure transmission medium (see for example Ref. 36 for more on silicon oil as a pressure transmission medium). The pressure at the sample position was determined by placing a small (0.5 mg) $(V_{0.99}Ti_{0.01})_2O_3$ crystal in the Teflon container for use as a manometer.[36] This material makes an excellent manometer as it displays a readily measurable metal-to-insulator transition which varies linearly in T with pressure for pressures of up to 10 kbar.[36]

The specific heat was measured using a standard thermal relaxation method in a Quantum Design Physical Property Measurement System (PPMS) above 2 K and a dilution refrigerator above 100 mK. For measurements below 2 K single crystals were polished flat and mounted on a Sapphire substrate with GE varnish. The opposite side of the 0.25-mm-thick sapphire substrate contained a RuO resistance thermometer which was notched to provide a thermometer-heater pair in good thermal contact with the sample. The thermometer was cycled from 300 to 4.2 K many times to ensure repeatability of the resistance at low temperatures.[37] The thermometer was calibrated by comparison to a Lakeshore calibrated germanium resistance thermometer. Four resistive wires provided electrical and thermal contact of the thermometer and heater to the mixing chamber of the dilution refrigerator. We carefully checked that the time constant for thermalization of all elements on the sapphire substrate was much smaller than the thermal time constant for thermalization to the cryostat at each measurement temperature. Specific heat measurements were carried out in magnetic fields between 0 and 6 T with all thermometers calibrated at each magnetic field. The specific heat of the addenda was measured separately and carefully subtracted from the data.

III. OVERVIEW OF EXPERIMENTAL RESULTS

A. dc susceptibility and magnetization measurements

In order to establish the magnetic ground states and critical temperatures of the $Fe_{1-x}Co_xS_2$ chemical substitution series we have measured the dc magnetic susceptibility, χ_{DC}, and magnetization, M, of our crystals. In Fig. 2 we plot χ_{DC} of a dozen representative samples with x ranging from nominally pure FeS_2 to $x=0.055$. Our $x=0$ crystal has a diamagnetic susceptibility that changes little as a function of temperature. The small size of the impurity related Curie-Weiss contribution to the susceptibility of this crystal observable below 20 K, an increase in 10^{-6} from 20 K down to 2 K, is consistent with an impurity concentration of 3×10^{18} cm^{-3}. Not only does this establish the quality of our pyrite crystals, it is compelling because it reaffirms that the parent compound is nonmagnetic despite being 1/3 iron.[13,14] The low-temperature χ_{DC} systematically increases with x by over 4 orders of magnitude for our $x=3 \times 10^{-4}$ to our $x=0.055$ samples. At the same time, the T dependence changes from being almost Curie-like at low x, to displaying a broad, almost constant region of χ_{DC} below 5 K for $x>0.035$. At higher temperatures χ_{DC} is less systematic in x with some crystals displaying almost constant χ_{DC} above 100 K suggestive of a significant Pauli susceptibility, while others show a more T-dependent χ_{DC} to higher temperatures crossing through χ_{DC} of samples with smaller x. Because the Pauli susceptibility is proportional to the conduction electron density of states, we interpret the variation in our measured χ_{DC} above 100 K as revealing a carrier density and, perhaps, a mass that is highly sensitive to the disorder. Because of this change from a systematic low-temperature χ_{DC} to a less systematic high-T χ_{DC}, we conclude that in the two temperature ranges χ_{DC} is dominated by two different electron populations; a more local population of electron moments dominates at low T while the more itinerant electrons dominate χ_{DC} at $T>100$ K.

To gain insight into the character of the magnetic moments responsible for the low T upturn in χ_{DC} we have plot-

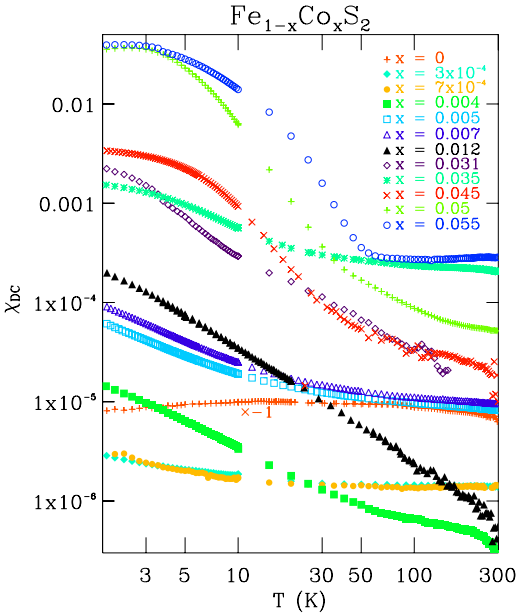

FIG. 2. (Color online) dc magnetic susceptibility. Temperature, T, and cobalt concentration, x, dependence of the dc magnetic susceptibility for several representative crystals. Note that the data for the $x=0$, nominally pure sample, is diamagnetic and thus has been multiplied by -1 for display purposes. Magnetic fields applied include 10 kOe for the $x=3\times10^{-4}$, 7×10^{-4}, and 0.004 crystals; 2 kOe for the $x=0$, 0.012, and 0.035 crystals; 1 kOe for the $x=0.005$, 0.007, and 0.045 crystals; and 50 Oe for the $x=0.031$, 0.05, and 0.055 crystals. Measurement fields were chosen so that noise levels were acceptable given the size of the susceptibility signal for each individual crystal.

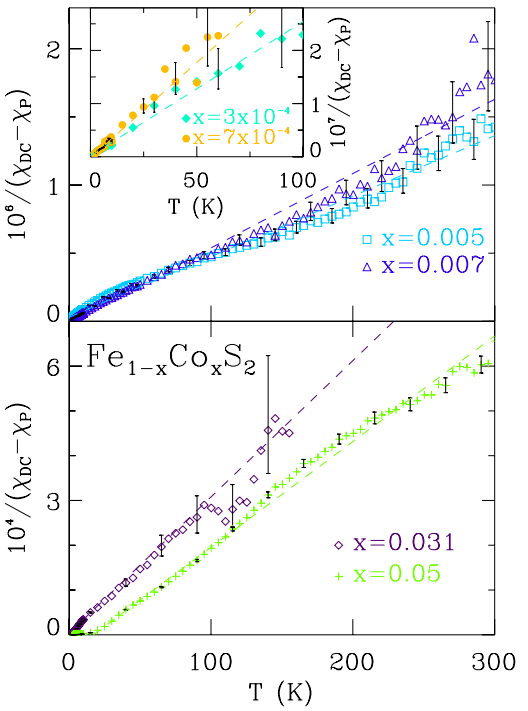

FIG. 3. (Color online) Inverse dc magnetic susceptibility. (a) and (b) Temperature, T, and cobalt concentration, x, dependence of the inverse dc magnetic susceptibility, $1/\chi_{DC}$, after subtraction of the temperature independent contribution, for several representative samples at the same magnetic fields as in Fig. 2. The constant susceptibility is attributed to the Pauli susceptibility, χ_P of our crystals. Inset to frame (a) displays $1/(\chi_{DC}-\chi_P)$ below 100 K for our $x=3\times10^{-4}$ and $x=7\times10^{-4}$ samples where the signal to noise level is such that Curie behavior is apparent in an inverse susceptibility plot. Error bars are plotted only for every fifth (third in inset) data point for display purposes.

ted in Fig. 3 the inverse dc magnetic susceptibility after subtraction of the temperature independent Pauli susceptibility, χ_P, $1/(\chi_{DC}-\chi_P)$ as a function of T. The Pauli susceptibility was determined from fits to the data in Fig. 2 at $T>20$ K by a model which included a Curie-Weiss term and a temperature independent constant and was assumed to be equal to the T-independent term. χ_P estimated in this manner is within error of the susceptibility at 300 K in Fig. 2. This is standard procedure for comparing the susceptibility data to a Curie-Weiss form, $\chi=CC/(T-\Theta_W^{DC})$ where CC is the Curie constant and Θ_W^{DC} is the Weiss temperature. Although some nonlinearity is apparent in the data, we have quantified the Curie-Weiss behavior by fitting a linear T dependence to the data as shown in the figure. We interpret the intercept of the fits with the T axis as Θ_W^{DC} and the slope as $1/CC$ where $CC=n(g\mu_B)^2J(J+1)/3k_B$ with n the density of magnetic moments of size J, g the gyromagnetic factor, k_B Boltzmann's constant, and μ_B the Bohr magneton. Both Θ_W^{DC} and CC are observed to increase systematically with x as can be seen in Fig. 4 where we plot the best-fit values of the quantity $ng^2J(J+1)=3CCk_B/\mu_B^2$ and Θ_W^{DC}. It is also interesting to note that for small x, $x<0.01$, Θ_W^{DC} is less than zero revealing a small antiferromagnetic interaction of the moments for small Co doping. This is perhaps not expected since at only slightly larger Co concentrations a disordered ferromagnetic ground-state results.

We note that the Curie constant increases with x beyond what would be expected for paramagnetic spin-1/2 magnetic moments for all samples measured. If we assume that the density of magnetic moments is equal to the Co density and that $g=2$ we would conclude that the magnetic moment increases from just above $J=0.5$ to between $J=1$ and 2 for $x\geq0.03$. This is the first indication that the magnetic moments likely form strongly interacting clusters over the temperature scale where the Curie constants were determined. The measured Curie constant, in this case, most likely reflects the fluctuations of a smaller density of much larger composite magnetic moments.

The magnetic properties of our samples was further explored by measuring M at 1.8 K in fields of up to 5 T. Figure 5(a) displays the enormous increase in M with x for a range of x between 3×10^{-4} and 0.085. In Fig. 5(b) we display M, in μ_B per Co dopant, to demonstrate the normalization used to determine the Co density of our crystals. The form of the magnetization can be seen to evolve from that of a Brillouin function, B_J, at small x to that of a ferromagnetically ordered material at larger x.

The temperature and field dependence of M, such as that shown in Fig. 5, is commonly compared to a mean-field form to determine T_c of magnetic materials. In Fig. 6 we display this comparison of $M(H,T)$ for two representative samples. The mean-field form for M is typically written as $M(H)$

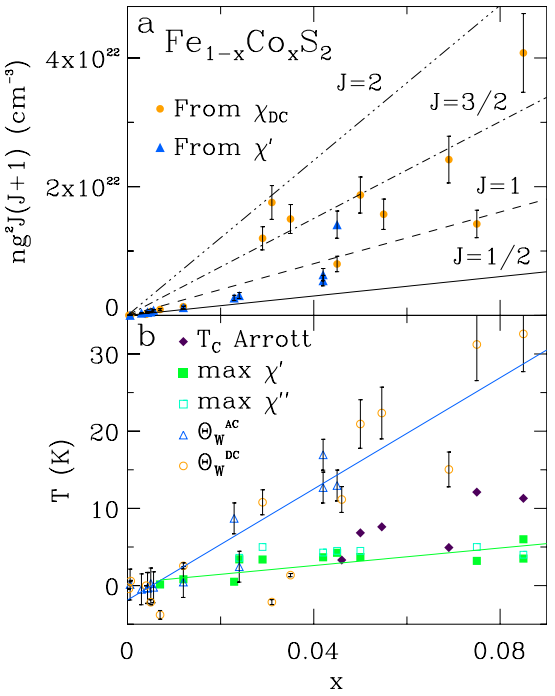

FIG. 4. (Color online) Curie constant, Curie temperature, and Weiss temperature. (a) The Curie constant, $ng^2J(J+1)$, determined from fits of a Curie-Weiss form added to a temperature independent Pauli contribution, χ_P, $\chi=n(g\mu_B)^2JJ(+1)/3k_BT+\chi_P$, to the dc and ac magnetic susceptibility. Lines indicate values of the Curie constant for various J's when n is set equal to the cobalt concentration of the crystals and g is set equal to 2. (b) The Curie temperature, T_C as defined by the temperature of the maximum in the real part of the ac susceptibility, max χ', and through a mean-field Arrott analysis, T_C Arrott (see text for details). The temperature of the maximum in the imaginary part of the ac susceptibility, max χ'' is included in the figure for comparison to max χ'. Weiss temperatures as determined from the temperature dependence of the ac, Θ_W^{AC}, and dc, Θ_W^{DC}, susceptibility are also plotted. Lines are fits of a linear max $\chi'(x)$ and $\Theta_W^{AC}(x)$ dependence to the data.

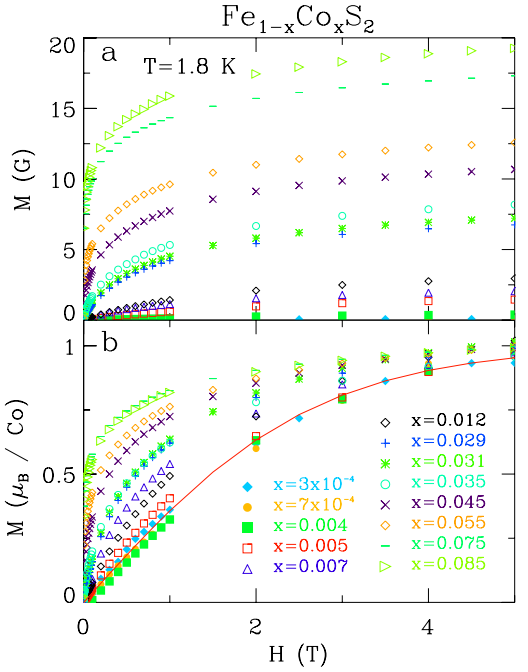

FIG. 5. (Color online) Magnetization. (a) The magnetization vs external magnetic field H at 1.8 K for several of our crystals with Co concentrations identified in frame b. (b) The magnetization normalized so that the high field values approach 1. This normalization was used along with the EDX data to determine x. The red line is a Brillouin function for $J=1/2$ and a gyromagnetic ratio of 2.

$=ngJ\mu_BB_J[gJ\mu_B(H+\eta M)/k_BT]$ with η the constant parameterizing the strength of the molecular mean field. From this starting point an expansion for H/M can be written as $H/M=(1/\chi_0)+aM^2+bM^4+\ldots$ where χ_0 is the initial susceptibility $[\chi(H=0)]$. Thus, a plot of M^2 vs H/M should be a straight line for a range of fields such that the higher terms can be ignored.[38] This is commonly referred to as an Arrott plot and is demonstrated by Fig. 6 frames a and b showing the results of such an analysis for two samples near the critical Co concentration for ferromagnetism. It is clear that the region of linearity of M^2 in H/M is limited, particularly at low temperatures. Frame c of the figure displays a compilation of $1/\chi_0$ values determined from the linear fits, such as those in frames a and b. We have plotted the values of $1/\chi_0$ vs T^2 since the Stoner-Wohlfarth theory of itinerant magnetism predicts a T^2 dependence of $1/\chi_0$ near the transition temperature. Linear fits to the low-T data are used to determine the T^2 intercept and this is interpreted as the mean-field T_c. The values for T_c determined in this way are plotted in Fig. 4(b) for comparison to Θ_W^{DC}. Modified Arrott analysis's having different dependencies of H/M on M were also performed without significant changes to the critical temperatures determined from the above analysis.[38] The conclusion from this mean-field analysis is that the Curie temperature is less than $1/2\Theta_W^{DC}$ for these samples reflecting the importance of disorder on the formation of the magnetic state and that there is a critical Co concentration for ferromagnetism near $x=0.03$. However, a simple mean-field analysis is likely to be inaccurate when T_c is close to zero.

B. ac susceptibility measurements

Although the dc susceptibility and magnetization give us a good initial indication of the formation of a ferromagnetic phase with the substitution of Co for Fe in FeS_2, the very subtle changes that occur near x_c are best explored at very low magnetic fields where good quality dc magnetization signals are difficult to obtain. Therefore, we have made very careful ac susceptibility measurements of our crystals using excitation fields of 1.5 Oe or less as shown in Fig. 7. In agreement with our dc results, the ac susceptibility shows a dramatic increase with x. However, there are two important differences between our dc and ac susceptibility apparent in the figures. First, the real part of the ac susceptibility, χ', is noticeably larger than χ_{DC} for all $x>0$ crystals measured. Second, distinct maxima appear in both χ' and, at slightly higher T's, the imaginary part of the ac susceptibility, χ'', as can be seen in frames a and b. As is common practice, we preliminarily interpret the temperature of the maxima in χ' as the critical temperature, T_c, for the development of a magnetic, ferromagnetic or spin glass phase. In Fig. 4(b) we plot

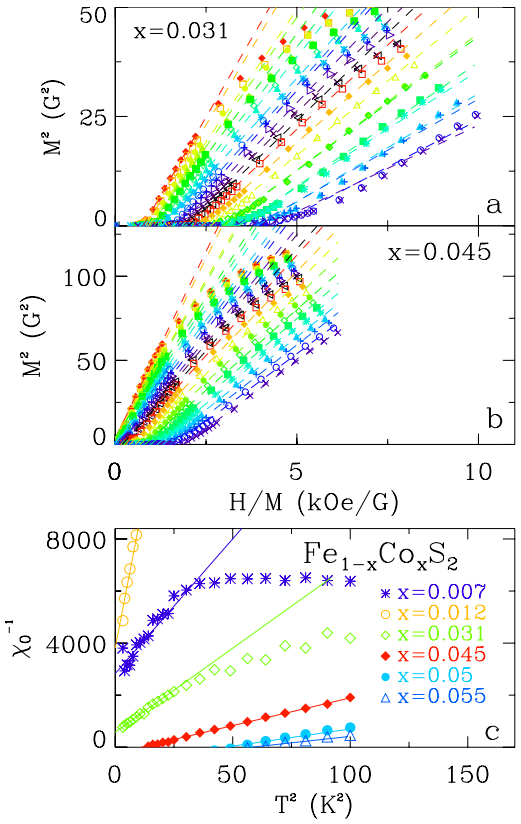

FIG. 6. (Color online) Arrott plots. Standard mean-field analysis for determining the Curie temperature, T_c, of ferromagnetic materials. In (a) and (b) we plot the square of the magnetization, M, vs the external field, H, divided by M. T_c is the temperature where the extrapolation of the data to $H=0$ goes through 0. (a) Arrott plot for an $x=0.031$ crystal. Data are at temperatures of 1.8 (filled diamonds), 2.0 (squares), 2.25 (bullets), 2.5 (open triangles), 2.75 (filled squares), 3.0 (open diamonds), 3.25 (filled triangles), 3.5 (asterisks), 3.75 (circles), 4.0 (pluses), 4.25 (open right pointing triangles), 4.5 (X's), 4.75 (left open left pointing triangles), 5.0 (open squares), 5.5 (filled diamonds), 6.0 (open triangles), 6.5 (bullets), 7.0 (open diamonds), 7.5 (filled squares), 8.0 (asterisks), 8.5 (filled triangles), 9.0 (pluses), 9.5 (circles), and 10 K (X's). Dashed lines are linear fits to data between 1 and 15 kOe. (b) Arrott plot for an $x=0.045$ crystal. Temperatures and symbols same as in frame a. Dashed lines are linear fits to data between 1 and 20 kOe. (c) Plot of H/M axis intercepts, χ_0^{-1}, of the linear fits to data in frames a and b vs T^2 for several crystals identified in the figure. The intercepts of these data with the T^2 axis is interpreted as the mean-field T_c.

T_c determined in this manner (max χ') along with the temperature of the maximum in χ'' (max χ'') for comparison to our analysis of χ_{DC} and $M(H)$. In contrast to our χ_{DC} results, our very low-T measurements (down to 50 mK) reveal a peak in χ' for all crystals with $x \geq 0.007$ indicating that $x_c = 0.007 \pm 0.002$. The contrasting results in our ac and dc magnetic susceptibility indicate that the magnetic state of these crystals is extraordinarily sensitive to magnetic field as we explicitly demonstrate in Sec. V below.

In frame c of Fig. 7 $1/\chi'$ is plotted against temperature to display the Curie-Weiss-like behavior of χ'. Here, the general Curie-Weiss-like trend is displayed although significant nonlinearity and structure are also apparent in these data.

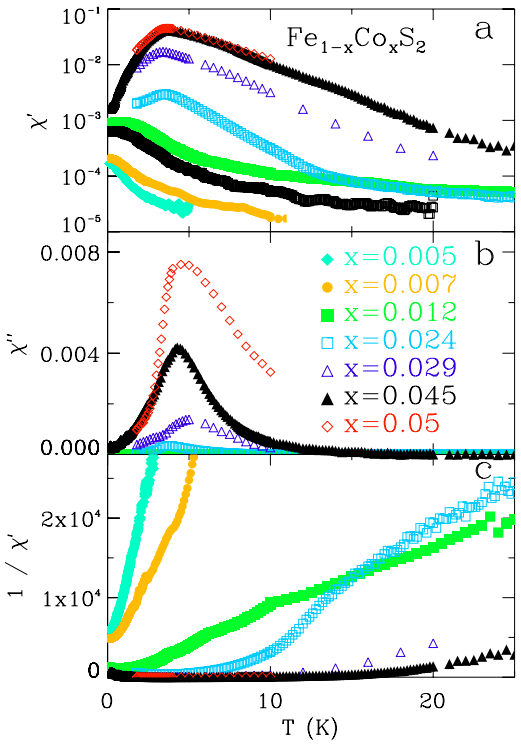

FIG. 7. (Color online) ac susceptibility. (a) The real part of the ac magnetic susceptibility, χ' of several of our crystals with Co concentrations identified in frame b. The ac excitation field was 1.5 Oe and the measurement frequency was 1.0 kHz for the $x=0.005$, 0.007, 0.012, 0.024, and 0.045 crystals, 1.0 Oe and 10 Hz for the $x=0.029$ crystal, and 1.0 Oe and 100 Hz for the $x=0.05$ crystal. (b) Imaginary part of the ac susceptibility, χ'', for the same crystals in frame a. Co concentrations are identified in the figure. (c) $1/\chi'$ demonstrating Curie-Weiss-like behavior. Data and symbols same as in frames a and b.

Linear fits of these data were used to determine the Weiss temperatures, Θ_W^{AC}, and Curie constants displayed in Fig. 4. There appears to be good compatibility of both Θ_W^{AC} with the values determined from the dc values, however, the Curie constant appears generally smaller for our ac analysis than for our dc values for $x>0.02$. The Curie constants determined from both methods indicate a fluctuating magnetic moment of $J>1/2$ per Co dopant indicative of magnetic cluster formation. Despite the general linear behavior of $1/\chi'$ well above T_c, there is a noticeable departure from this behavior at $T<4\Theta_W^{AC}$ that can best be seen for our $x=0.024$ sample in frame c of Fig. 7. Fits of $1/\chi'(T)$ for $T>15$ K indicate $\Theta_W^{AC}=3$ K, however, at $T<15$ K $1/\chi'$ tends toward much smaller values. This tendency for χ' to increase at a rate faster than the Curie-Weiss behavior indicates local ferromagnetism and further supports our observation that magnetic clusters form at temperatures above T_c. A more complete description of this behavior is presented in Sec. V of this paper.

The effect of hydrostatic pressure, P, on the magnetization of our crystals is demonstrated in Fig. 8. While the magnitude of χ' is depressed by the application of pressures of order of a kbar, there is little change to the temperature of the peak in χ'. The changes that occur with P are demonstrated

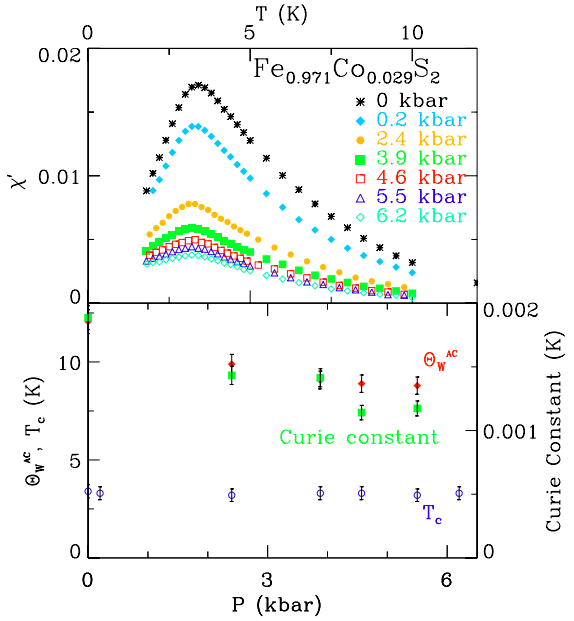

FIG. 8. (Color online) Pressure dependence of the ac magnetic susceptibility. (a) The pressure, P and temperature, T, dependence of the real part of the ac magnetic susceptibility, χ', for an $x=0.029$ crystal at zero dc magnetic field and at pressures identified in the figure. Data taken with an excitation field of 1 Oe at a frequency of 1 Hz. (b) Curie temperature, T_c, as defined by the temperature of the peak susceptibility in frame a, of our $x=0.029$ crystal as a function of P. Also shown are the Weiss temperature, Θ_W, and Curie constant derived from fits of the Curie-Weiss form to the real part of the ac susceptibility shown in frame a. Note: Θ_W and the Curie constant were determined only for pressures where sufficient $T>15$ K χ' data (not shown) was available.

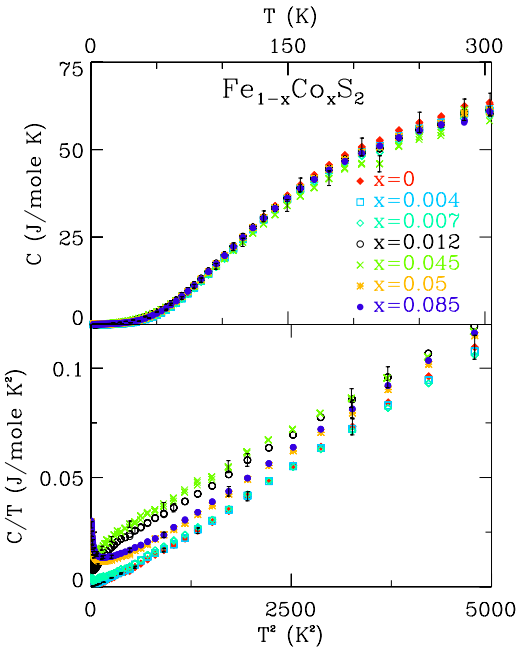

FIG. 9. (Color online) Specific heat. (a) The temperature, T, dependence of the specific heat, C for seven representative $Fe_{1-x}Co_xS_2$ crystals with x identified in the figure. (b) Specific heat divided by temperature, C/T, plotted as a function of T^2 for temperatures between 2 and 70 K. Symbols are the same as in frame a. Representative error bars are shown in both frames.

in frame b of the figure where the temperature of the peak in χ', taken as our definition of T_C, is plotted along with the results of fitting a Curie-Weiss form to $\chi'(T)$ above 15 K. Both the Curie constant and the Weiss temperature are reduced as P is applied showing that P reduces both the average size of magnetic clusters as well as the average interaction energies between magnetic moments evident in the $P=0$ measurements. The Curie constant shown in Fig. 8 is consistent with a reduction in the density of $J=1/2$ magnetic moments from 3×10^{21} to 1.7×10^{21} cm^{-3} as the pressure is increased from ambient to 6 kbar. Equivalently we can assume that the density of moments remains equal to the Co density and that the changes in the Curie constant reflect a reduction in J from 1.3 to 0.9 with P. Our data could also be interpreted as a general trend toward a stronger Kondo coupling with P as has been shown to be typical in the case of f-electron compounds.[39]

C. Specific heat and entropy

The specific heat, C of our crystals was measured to characterize the changes to the thermodynamic properties that occur upon Co doping FeS_2. As can be seen in Fig. 9, where C is plotted for seven representative crystals, there is little change in $C(T)$ with Co doping between 50 and 300 K. In frame b of the figure we concentrate our attention on the low-temperature specific heat where changes in the electronic contributions are apparent. Here we plot the data in the standard manner for characterizing the electronic contributions, $C(T)/T$ vs T^2, since in standard paramagnetic metals the specific heat is expected to be accurately described by a $C(T)/T=\gamma+\beta T^2$ form in the temperature range displayed. In this equation γ represents the coefficient of electronic specific heat and is proportional to the density of electronic states, while β parameterizes the phonon contribution to the specific heat at temperatures well below the Debye temperature. While $\beta=2.17\times10^{-5}$ J/mol K^4 describes the phonon contribution of all our samples well, there are significant changes to the electronic contribution to $C(T)$ with x. It is clear that γ of the nominally pure FeS_2 crystal is consistent with zero and that γ increases with x. However, there are contributions to the specific heat that are not described by the standard form. For example, at the lowest temperatures an upturn in $C(T)/T$ with decreasing T is apparent in all of the Co doped samples. Several of the data sets also show an increased contribution between 10 and 70 K that is not described by a simple constant. It is most likely that the differences from the standard metallic form are due to the formation of the magnetic ground state with Co doping that was apparent in the magnetic susceptibility.

We expand the low-$TC(T)/T$ data in Fig. 10 to highlight the changes that occur to the electronic contributions with increasing x. In this figure the changes in γ with x above 1 K are made clearer along with the large increases in $C(T)/T$ that occur below 1 K in the Co doped samples. The increases to γ with x are very large considering that Hall effect measurements estimate the carrier concentrations are only 10 to

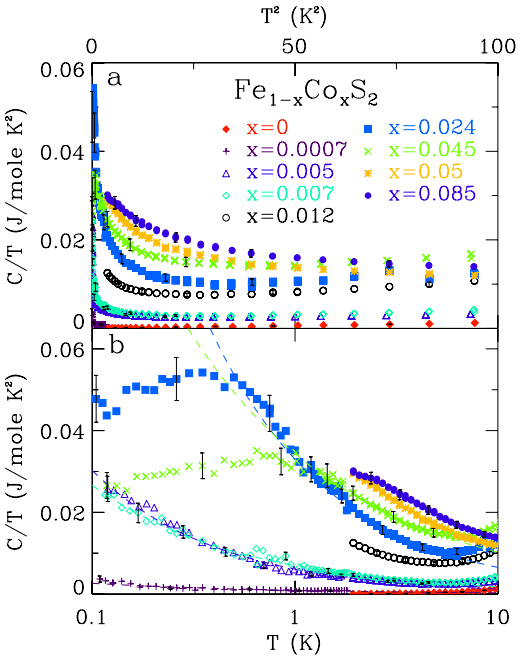

FIG. 10. (Color online) Low-temperature specific heat. (a) The specific heat divided by temperature, C/T, plotted as a function of T^2 below 10 K for nine representative crystals with x identified in the figure. Error bars are shown for a few representative data points. (b) Specific heat divided by temperature, C/T, plotted as a function of T on a logarithmic scale. Symbols are the same as in frame a. Error bars are shown for a few representative points. Dashed lines are fits of the form aT^{α_C-1} to the data with an α_C of -0.45 ± 0.05 for the $x=0.0007$, -0.70 ± 0.05 for the $x=0.005$, -0.60 ± 0.05 for the $x=0.007$, -0.70 ± 0.05 for the $x=0.024$, and -0.50 ± 0.05 for the $x=0.045$ crystals. Note that the temperature range for the fits was limited to $T>1$ K for the $x=0.024$ and $x=0.045$ crystals.

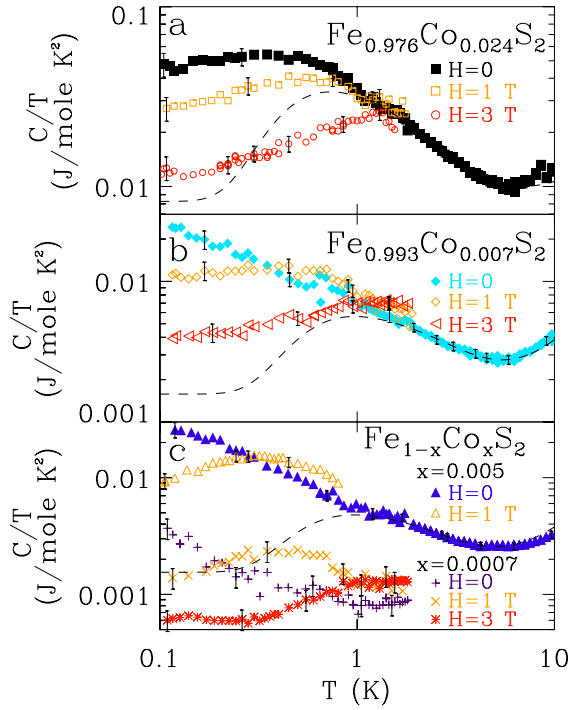

FIG. 11. (Color online) Magnetic field dependence of the low-temperature specific heat. (a) The magnetic field, H, and temperature dependence of the specific heat divided by temperature, C/T for an $x=0.024$ crystal at fields identified in the figure. Dashed line is a fit of the Schottky form (Ref. 45) for a collection of free magnetic moments in a magnetic field added to the phonon contribution to the specific heat determined by C of a nominally pure single crystal to the $H=0$ C/T data for $T>2$ K. This fitting procedure was carried out with the quantity $ng^2J(J+1)$ held constant at the value determined by fits of the Curie-Weiss form to the real part of the ac magnetic susceptibility measured on the same crystal. The fitting procedure resulted in best-fit parameters of the effective field, $H_{eff}=1.4$ T, a magnetic moment, $J=2.2$, and a density of magnetic moments, $N=9.5\times10^{19}$ cm^{-3}. (b) The H and T dependence of C/T of an $x=0.007$ single crystal at fields identified in the figure. Dashed line is a fit of the same form as in frame a to the $H=0$ data. Best-fit parameters were $H_{eff}=1.8$ T, $J=2.6$, and $N=2.0\times10^{19}$ cm^{-3}. (c) The H and T dependence of C/T of $x=0.005$ and $x=0.0007$ single crystals as identified in the figure at fields identified in the figure. Dashed line is the a fit of the same form as in frame a to the $x=0.005$, $H=0$ data. Best-fit parameters were $H_{eff}=1.88$ T, $J=2.4$, and $N=1.6\times10^{19}$ cm^{-3}. Error bars are shown for a few representative data points in each frame.

30% of the Co concentration in our samples.[12] Such a large density of electronic states is commonly interpreted as a large electronic effective mass. Our estimates for the carrier effective mass, m^*, from the $C(T)/T$ data above 5 K range from four times the bare electron mass, m_e, to over 40 m_e for samples with x just beyond x_c. If we were to consider the large upturn in $C(T)/T$ below 1 K to be electronic in origin, our estimates of m^* increase to values between 120 and 250 m_e at 120 mK. Heavy mass carriers are rare in transition metal compounds, however, several Fe-based semiconducting, or semimetallic, materials have been reported to have substantial carrier mass enhancement.[40,41] Crystals with $x<x_c$, as determined from the ac magnetic susceptibility, display a $C(T)/T$ that increases continuously down to the lowest measurement temperatures (0.1 K). Those with $x>x_c$ display a maximum in $C(T)/T$ at a temperature somewhat below T_c as determined from the temperature of the maximum in χ'.

In order to characterize the specific heat further, we have measured the magnetic field dependence of $C(T)/T$ as shown in Fig. 11 for 4 of our single crystals. For all four of the samples application of magnetic field decreases the low-temperature $C(T)/T$ while increasing slightly $C(T)/T$ above 1 K. This behavior is qualitatively similar to the changes that occur upon application of a magnetic field in simple doped semiconductors such as Si:P.[42] The low-T specific heat of Si:P has been modeled in terms of local moments induced by the doping that are thought to form singlets such that the ground state of the system has zero net moment.[43,44] The effect of disorder is to create a broad distribution of interactions between the local moments. As a result, $C(T)/T$ increases as a small power law at low temperatures.[44] However, we do not believe such a description to be relevant in the case of $Fe_{1-x}Co_xS_2$ since our crystals have a nearly ferromagnetic, or ferromagnetically ordered, ground state. Instead, we attribute the unusual temperature dependence of $C(T)/T$ as being due to the interaction of a random distribution of local moments together with the interaction of the local moments and conduction electrons. As the magnetic

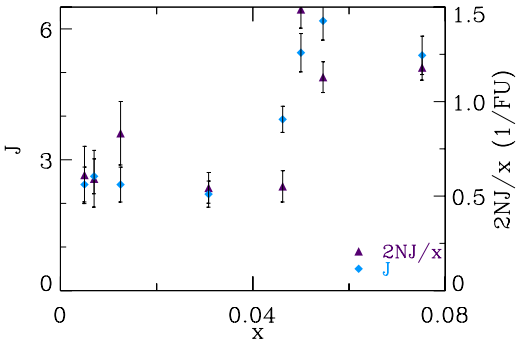

FIG. 12. (Color online) Magnetic moments from specific heat and susceptibility analysis. Magnetic moment, J, and the quantity $2NJ/x$ where N is the density of magnetic moments of size J per $Fe_{1-x}Co_xS_2$ formula unit determined from fits to the dc susceptibility and the specific heat above $T=2$ K as described in text.

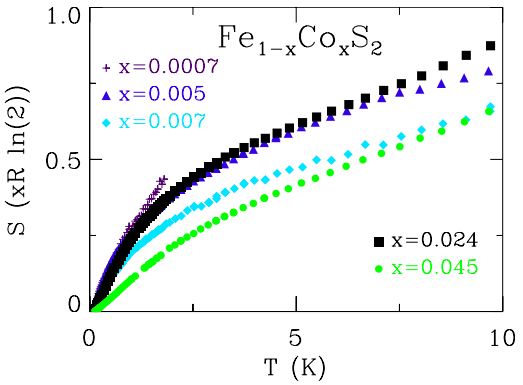

FIG. 13. (Color online) Entropy determined from the specific heat. (a) The temperature, T, dependence of the entropy, S, determined by numerical integration of the C/T data for five representative single crystals with stoichiometry's identified in the figure.

field is increased beyond the level of the interactions, $C(T)/T$ resembles a sum of contributions from a Fermi gas of electrons (a constant γ) and a separate contribution from effectively noninteracting magnetic moments. The contribution from noninteracting moments in a magnetic field is commonly referred to as a Schottky anomaly[45] and is demonstrated in the figure by the dashed lines. We note that above 1 K the specific heat in zero field is well described by this Schottky form added to a temperature independent γ and the phonon contribution taken as $C(T)/T$ of the nominally pure FeS_2 crystal.

We have checked that our conclusion of formation of ferromagnetic clusters of magnetic moments at low T is consistent with our $C(T)$ measurements by quantitatively comparing $C(T)/T$ and χ_{DC}. As we stated above, the large Curie constants seen in Fig. 4 are likely caused by the fluctuations of clusters of magnetic moments and both the specific heat and the magnetic susceptibility are sensitive to the density and size of the fluctuating moments. Therefore, we have fit the specific heat at $T>2$ K as shown in Fig. 11 with the Schottky form[45] discussed above for a set of noninteracting magnetic moments subjected to an effective molecular field. This contribution was added to a T-independent term representing a Fermi liquid of conducting electrons and the specific heat of the nominally pure FeS_2 crystal as a model of the contribution to $C(T)$ from phonons. For this fitting procedure we have held the quantity $ng^2J(J+1)$ constant at the value determined by $\chi_{DC}(T)$ and calculated the best-fit values of the effective molecular field, H_{eff}, J, and n. In Fig. 12 we present the results, plotting the best-fit values of J, which varied from less than three to six across our range of x, and the parameter $2NJ/x$ where $N=n/n_{FU}$ and n_{FU} is the density of $Fe_{1-x}Co_xS_2$ formula units. We plot the quantity $2NJ/x$ to check our assumption that each Co dopant donates a local magnetic moment of $s=1/2$ to FeS_2. A value of $2NJ/x=1$ corresponds to agreement with this assumption and although there is significant scatter in Fig. 12, there is general agreement. The best-fit values of H_{eff} varied between 1.4 and 2.6 T. We conclude that both χ' and $C(T)/T$ above 2 K are consistent with fluctuating magnetic moments whose size is several times larger than the magnetic moment of a single noninteracting Co dopant in an FeS_2 lattice. We note, however, that the simple mean-field forms we employ in this analysis are not sufficient to account for the interactions of moments within the clusters. Thus, the values plotted in Fig. 12 are rough estimates of the average cluster sizes.

The conclusion of magnetic cluster formation was further explored by calculating the entropy, $S(T)$, from C according to the relation $\int_0^T C(T')/T'dT' = S(T)$ for the small number of crystals that we have measured below 1 K. We have subtracted the phonon contributions to $C(T)$ prior to performing the integrations and the result of this procedure is shown in Fig. 13. Here S approaches $xR\ln(2)$ only for temperatures well above 10 K. Thus, there is significant entropy missing at 10 K consistent with the idea that clusters of spins form at temperatures of this order. Taking the entropy at 7 K as a benchmark allows us to estimate the average cluster size at this temperature. We make use of the form $S=(x/k)R\ln[2(k/2)+1]$ where k is the average cluster size of spin 1/2 moments, presumably localized on Co sites, to make the estimate. We find average cluster sizes that range from about three to five for the samples where data below 1 K are available. If we assume an exponentially decaying probability for clusters containing N spin-1/2 Co impurities, we estimate that about 10% of the cluster sizes will contain 10 or more spins at this T. The reduction in entropy below $xR\ln 2$ with cooling evident in Fig. 13 implies long ranged interaction between the local magnetic moments induced by Co substitution. For these Co concentration levels and assuming that Co ions are substituted randomly for Fe atoms in the FeS_2 crystal structure, we calculate that the average distance between impurity sites to be at the level of third nearest neighbors. Thus we estimate the range of interactions between the magnetic moments to be at least 1 nm in order to produce the reduction in entropy we observe below 10 K, as well as the formation of magnetic clusters apparent in the magnetic susceptibility to somewhat higher T.

In addition, the changes in the entropy that occur with magnetic field can be viewed in Fig. 14. The sensitivity of $C(T)/T$ and S to magnetic fields confirms the magnetic origin of the specific heat in this temperature range. For very small x, $x=7\times10^{-4}$ for example, increases in S are observed below 2 K for $H=1$ T, a sign that there is still a significant

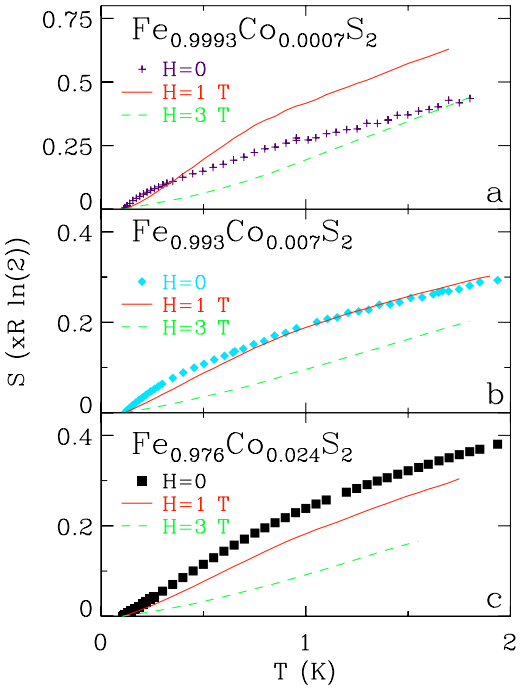

FIG. 14. (Color online) Field dependence of the entropy determined from the specific heat. The temperature, T, dependence of the entropy, S, determined by numerical integration of the C/T data at magnetic fields, H identified on the figure for (a) an $x=7\times10^{-4}$, (b) an $x=0.007$, and (c) an $x=0.024$ crystal.

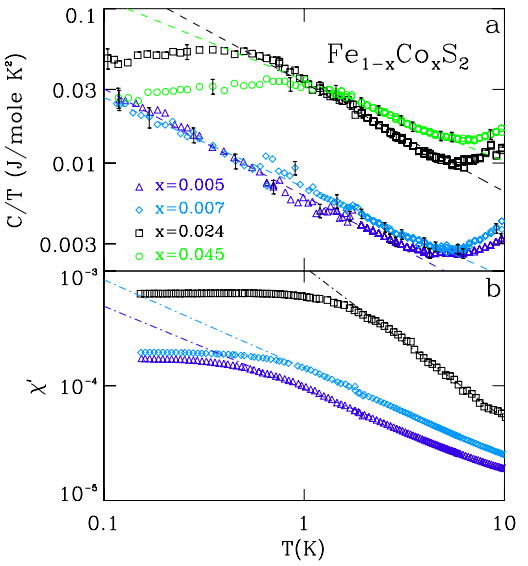

FIG. 15. (Color online) Low-temperature specific heat and magnetic susceptibility. (a) The temperature dependence of the specific heat divided by temperature, C/T for several representative crystals with x identified in the figure. Error bars are shown for a few representative data points. Dashed lines are fits to C/T to a power-law form, $C(T)/T \propto T^{\alpha_C-1}$ as in Fig. 10. (b) real part of the ac magnetic susceptibility, χ' for the same crystals as in frame a. Symbols the same as in frame a. dashed dotted lines are fit of a power-law form to χ', $\chi' \propto T^{\alpha_\chi-1}$ with exponents, α_χ of 0.25 ± 0.1 for the $x=0.005$, 0.22 ± 0.1 for the $x=0.007$ and -0.3 ± 0.2 for the $x=0.024$ crystals.

contribution to the entropy that we are not accessing because it lies below our lowest measurement temperature. Thus, for small x, there is a significant density of magnetic moments that interact with energy scales of less than 100 mK. At larger x, $x\geq0.007$, a suppression of S with field is observed from which we conclude that there are very few magnetic moments with such small energies of interaction. This is consistent with our conclusion that there is significant cluster formation in these samples at temperatures above those accessed in Fig. 14 and for our $x=0.024$ sample, a peak in χ' at 0.5 K that we associate with a disordered ferromagnetic transition.

IV. GRIFFITHS BEHAVIOR NEAR THE CRITICAL CONCENTRATION

As we noted in our previous discussion of both the ac and dc magnetic susceptibility, the Curie constants determined from simple fits to the temperature dependence were larger than is to be expected for paramagnetically fluctuating spin-1/2 magnetic moments. That is, the Curie constants displayed in Fig. 4 lie systematically above the solid line representing the Curie constant expected when each Co dopant donates a fluctuating $J=1/2$ magnetic moment. If we focus our attention on those samples closest to x_c, we find Curie constants 1.5 to 1.75 times larger than the simple estimate based on the expectation that each Co dopant adds a single spin-1/2 moment and the Curie law, $\chi(T)=CC/T$ with $CC=g^2\mu^2nJ(J+1)/3k_B$. This is an indication that FM ordered clusters of magnetic moments are forming below 100 K, where the Curie behavior becomes evident for this dopant concentration. With the assumption that the magnetic moments are coupled ferromagnetically, the size of the Curie constant would indicate that on average each cluster contained between 2.5 and 3.2 spin-1/2 magnetic moments for $x\sim x_c$. In addition, we have checked that this estimate is consistent with $C(T)$ above 2 K where the data can be interpreted in terms of a Schottky anomaly associated with entropy of fluctuating magnetic moments. This rough estimate of the average size of fluctuating magnetic clusters is further supported by estimates made from the entropy determined from the integral of $C(T)/T$ (Fig. 13).

Motivated by theoretical predictions about the importance of rare regions in disordered magnetic systems,[19,20] we have carefully examined the temperature and field dependent behavior of the magnetization and specific heat of our samples with x in proximity to x_c to search for such effects. We are not disappointed in that unusual behavior is discovered. The clearest indication of the importance of rare large clusters of magnetic moments comes from the temperature dependence of the specific heat below 1 K shown in Fig. 10(b). Here $C(T)/T$ is seen to increase without any suggestion of saturation down to 0.1 K for our samples closest to x_c, $x=0.005$ and 0.007. As indicated by the quality of the fits of a power-law form, represented by the dashed lines in the figure, as well as the linearity of the data when plotted on a log-log scale in Fig. 15(a), these data are well represented by a $C(T)\propto T^{\alpha_C-1}$ form with α_C between 0.3 and 0.45 for over a decade in T. Similar power-law behavior is observed in χ' over the same temperature range for the same crystals as can

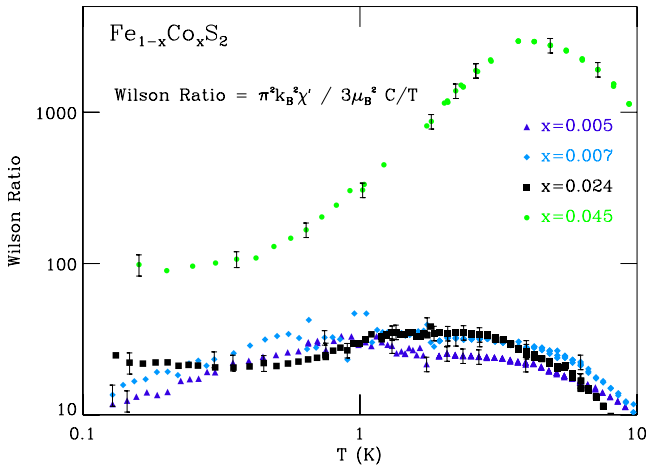

FIG. 16. (Color online) Wilson Ratio. The Wilson ratio, $\pi^2 k_B^2 \chi'/3\mu_B^2 C/T$, for crystals with x identified in the figure.

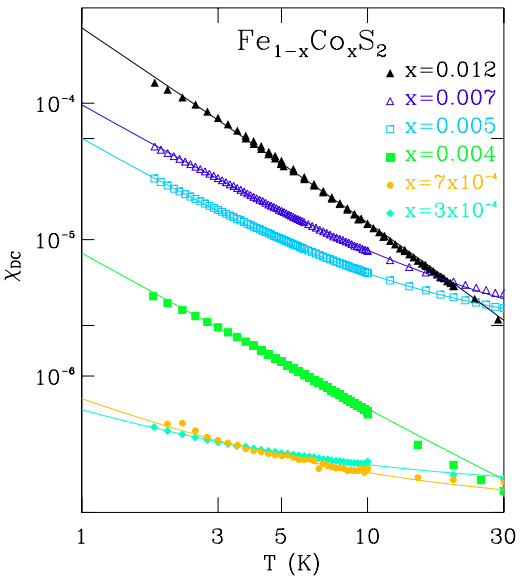

FIG. 17. (Color online) Power-law temperature dependence of the dc magnetic susceptibility. The dc magnetic susceptibility, χ_{DC}, vs temperature, T for crystals with $x \leq x_c$ as identified in the figure. Data is the same as that shown in Fig. 2. Lines are fits to the form $\chi_{DC}=\chi_c+CC/T^{\alpha_{DC}-1}$ as described in the text.

be seen in Fig. 15(b). Here χ' is well fit by a $T^{\alpha_\chi-1}$ form between 0.8 and 10 K with α_χ between 0.2 and 0.25 for these samples. We note, however, that χ', unlike $C(T)/T$, tends to saturate below 0.5 K.

We make a direct comparison of the real part of the ac magnetic susceptibility with $C(T)/T$ in Fig. 16 where the Wilson ratio, defined as

$$\pi^2 k_B^2 \chi'/3\mu_B^2 C(T)/T, \tag{1}$$

is shown. In this figure we observe that the two samples with x close to x_c have a Wilson ratio somewhat larger than 10. This value is similar to that observed near the critical point for magnetic ordering in $CePd_{1-x}Rh_x$ which is thought to enter a Kondo-cluster-glass phase and has properties compatible with the quantum Griffiths phase scenario.[46] Estimates for the average sizes of the fluctuating magnetic moments from the Wilson ratio of $Fe_{1-x}Co_xS_2$ yield about 3 to 4 spins consistent with our other estimates.[19] We note that the Wilson ratio at the lowest temperatures is not constant, but instead retains a slight temperature dependence reflecting the observation that at low-T $C(T)/T$ continues to display a power-law temperature dependence whereas χ' tends to saturate. We note that predictions of the Wilson ratio in Griffiths phases models indicate a weak, logarithmic, temperature dependence.[19] For our samples with $x > x_c$ the Wilson ratio becomes very large exceeding 1000 near T_c indicating a strong ferromagnetic tendency.

In addition, our finite-H dc magnetic susceptibility measurements indicate a small power-law temperature dependence below 10 K as can be seen in Fig. 17. Although the temperature range is restricted, for samples with $x < x_c$ a fit of the form $\chi_{DC} \propto T^{\alpha_{DC}-1}$ results in small, between 0.4 and 0.05, values of α_{DC}. We note that these data were taken in significant dc magnetic fields of between 1 kG and 1 T in order to produce reasonable signal sizes for our SQUID magnetometery measurements. Even so, we find similar small power-law behavior with the tendency for α_{DC} to fall toward zero near x_c. A compilation of the power laws determined from these different measurements is presented in Fig. 18 where some scatter in the values is apparent along with the tendency for larger α values to be found in specific-heat measurements than in magnetic susceptibility measurements.

Our data and analysis outlined above have led us to the conclusion that ferromagnetic clusters form at $T > T_c$. The sensitivity of our susceptibility measurements to small increases in pressure is one of the consequences of these weakly interacting ferromagnetically coupled clusters. In addition, we observe small power-law dependencies of $C(T)/T$, χ', and χ_{DC} at low T with changes in temperature as was demonstrated in Fig. 15 for χ', in Figs. 10 and 15 for the specific heat, and is apparent in Fig. 17 for χ_{DC}. In each case these quantities are observed to vary as $T^{\alpha-1}$ with $0 < \alpha < 0.6$. All of these power laws have similar values although there is significant scatter apparent. However, the similarities between these power laws, α_M, α_{DC}, and α_C for individual samples implies that a single physical mechanism may be responsible.

A clue as to the identity of the physical mechanism can be found in the dependence of the magnetization on temperature and magnetic field, $M(T,H)$. As we have noted above, the magnetic susceptibility does not conform to Curie-Weiss dependence, instead being characterized by a smaller power-law divergence at low T. This T dependence suggests a magnetization that is caused by independent fluctuators having a power-law local energy distribution, $P(\Delta) \sim \Delta^{\xi-1}$, where Δ is the local energy scale of the fluctuator. The form of the magnetization for freely fluctuating paramagnetic moments is well known to follow the Curie law $M(T,H) = ng\mu_B J B_J(g\mu_B H/k_B T)$, where B_J is the Brillouin function[47] and thus scales as $M(T,H) \propto F(H/T)$. In the case of the power-law energy distribution the magnetization has been shown to scale as $M(T,H) = H^\xi F(H/T)$.[19] As can be seen in Fig. 19(a), which displays $M(T,H)$ between 1.8 and 10 K for our two crystals with x closest to x_c, the standard scaling

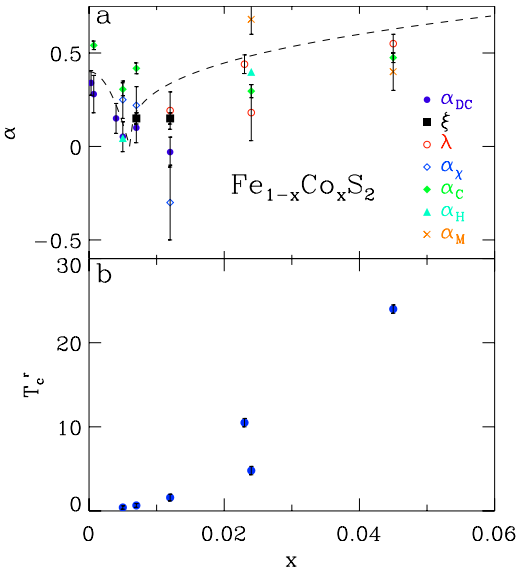

FIG. 18. (Color online) Results of power-law fits to the magnetic susceptibility and specific heat. (a) The best-fit exponents from fits of simple power-law forms to the ac and dc susceptibility and specific heat, C, temperature, T, and magnetic field, H, dependence above the Curie temperature of $Fe_{1-x}Co_xS_2$ for $3\times10^{-4}\leq x\leq0.055$. Here α_{DC} is the temperature exponent from fits of the form $\chi_{DC}=cT^{\alpha_{DC}-1}$ to the dc magnetic susceptibility data below 10 K, ξ determined from a scaling of $M(T,H)$ data described in the text, λ taken from fits of Eq. (2) to the T dependence of the real part of the ac susceptibility, χ', α_χ is from fits of χ' to the form $\chi'=cT^{\alpha_\chi-1}$ between 0.8 and 10 K, α_C taken from fits of the form $C/T=cT^{\alpha_C-1}$ to the T dependence of the specific heat, α_H taken from fits of the form $C/T=cH^{\alpha_H-1}$ to the H dependence of C/T, and α_M is taken from fits of the form $\chi'=cH^{\alpha-1}$ to the H dependence of χ'. Dashed line is a guide-to-the-eye. (b) Plot of the temperature characterizing the maximum interaction between magnetic moments, T_c^r taken from fits of Eq. (2) to the T dependence of χ' for $T>T_c$.

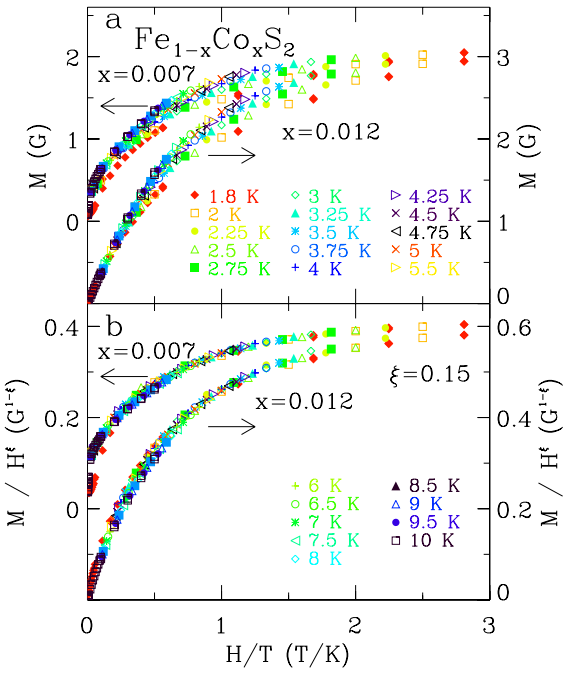

FIG. 19. (Color online) Scaling plot of the magnetization. (a) Plot of the magnetization, M, of $Fe_{1-x}Co_xS_2$ crystals with $x=0.007$ (left side scale) and $x=0.012$ (right side scale) as a function of magnetic field, H, divided by temperature T, (H/T) to display the quality of the standard paramagnetic scaling form $M(T,H)\propto F(H/T)$. Constant temperature, T, sweeps are shown for T's indicated in the frame and in frame b for $1.8\leq T\leq10$ K for $0\leq5$ T. (b) Plot of the same $M(T,H)$ data as in frame a, divided by H^ξ as a function of H/T. Reasonable scaling of the data is achieved for $\xi=0.15\pm0.05$.

form does not scale our data satisfactorily. This is to be expected for a system on the verge of magnetic ordering where magnetic moments have significant interaction. However, by simply allowing for a small value of ξ we can scale all of our H and T dependent data reasonably well as can be seen in frame b of the figure ($\xi=0.15$). We note that ξ is smaller than the values we found for α_C and α_{DC}, but still distinct from zero. We note that this form for M does not hold well for $x>0.04$ since $M(H)$ increases sharply at low fields thus resembling more closely $M(H)$ of ferromagnetic materials.

In addition to this unusual field and temperature dependence of M, our specific-heat measurements also reveal a strong sensitivity to magnetic fields as we demonstrated in Fig. 11. Although we found that above 2 K the T and H dependence of C/T appears consistent with a Schottky anomaly form, C/T below 1 K is not, even when a 3 T magnetic field is applied. This is emphasized by the magnetic field dependence of the low-T specific heat which is explicitly displayed for $T=120$ mK Fig. 20. Here moderately sized fields are seen to suppress $C(T)/T$ dramatically. The power-law-like decrease in $C(T)/T$ is displayed in the inset where the lines are powerlaws in field, $C(T)/T\propto H^{\alpha_H-1}$ with $\alpha_H=0$ for the $x=0.005$ crystal and 0.4 for the $x=0.024$ crystal. We note that for a Schottky anomaly $C(T)/T$ decreases exponentially in H for fields where $g\mu_BH>k_BT$ which is inconsistent with our data.[45]

Although there are many physical realizations of this scaling form for the magnetization we observe (independent fluctuators with a power-law energy distribution) and small power-law T dependent magnetic susceptibilities have been known to describe doped semiconductors very near insulator-to-metal transitions, our identification of magnetic clusters forming in this doped semiconducting system presents an obvious candidate explanation for all of the data presented thus far. We posit that our data lead naturally to the conclusion that Griffiths phase formation is the most likely physical mechanism responsible for the unusual properties we measure for samples in proximity to the critical concentration for magnetic ordering.

Magnetic Griffiths phenomena have been used to describe disordered magnetic systems theoretically in the case where the disorder is sufficient to cause inhomogeneity in the formation of the magnetic ground state.[18] In the vicinity of the quantum critical point, droplets of the magnetically ordered phase are thought to form due to the inhomogeneities inherent to a chemically substituted material. These droplets reside within the paramagnetic phase and can be exponentially rare if the statistics are Poissonian so that $P(V)\sim e^{-cV}$, where P is the probability of having a droplet of volume V and c is

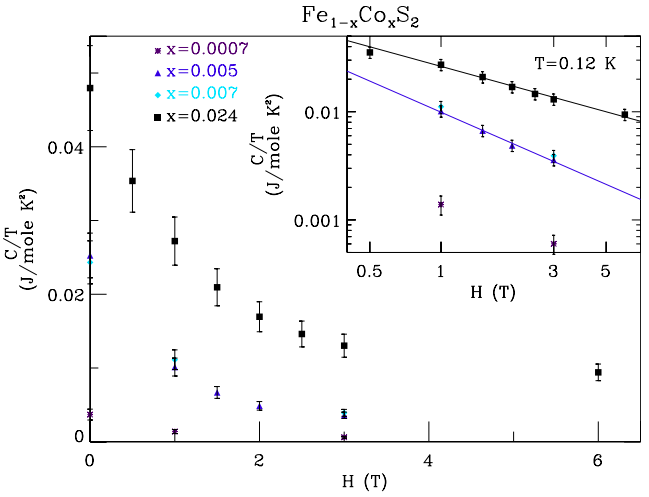

FIG. 20. (Color online) Magnetic field dependence of the specific heat at $T=0.12$ K. The magnetic field, H, dependence of the specific heat divided by temperature, C/T for several crystals with stoichiometry's identified in the figure. Inset: The same $C(T,H)/T$ data plotted with logarithmic axes. The lines are fits of a power-law form to C/T data for the $x=0.005$ and 0.024 crystals. Best-fit values of the exponents are -1 for the $x=0.005$ crystal and -0.6 for the $x=0.024$ crystal.

related to the strength of the disorder.[19] Since $Fe_{1-x}Co_xS_2$ has a ferromagnetic ground state for $x>x_c$, the droplets most likely carry a net magnetic moment simply proportional to the size of the droplet. These magnetic moments will have a finite probability of tunneling to nearby excited magnetization states. The tunneling rate for such a droplet is predicted to be exponential in the number of spins that form the droplet such that $\Delta \sim \omega_0 e^{-bV}$ where b is a constant related to the microscopic tunneling mechanism and ω_0 is a frequency cutoff.[19] Since the tunneling rate is proportional to the energy splitting of the different magnetization states the distribution of energy splittings can be written as $P(\Delta) \sim \int dV P(V) \delta[\Delta - \omega_0 e^{-bV}] \sim \Delta^{\xi-1}$, where $\xi=c/b$, giving us our power-law distribution of energy levels suggested by the scaling of our $M(T,H)$ data. With this form for the energy splittings, power-law forms for the magnetic susceptibility and specific heat follow by considering all clusters with $\Delta > k_B T$ to be frozen such that they do not contribute to the susceptibility or entropy.[19] Thus, a modified Curie form $\chi'(T) \propto n(T)/T$, where $n(T)$ is the density of clusters with $\Delta < k_B T$ is predicted.[19,20] $n(T)$ can be easily calculated from $P(\Delta)$ as $n(T) \propto \int_0^T P(\Delta) d\Delta \propto T^\alpha$ and thus, $\chi'(T) \propto T^{\alpha-1}$. In addition, $S(T) \propto n(T) R \ln(2J+1) \propto T^\alpha$ and since $C(T)/T = dS/dT$ we have $C(T)/T \propto T^{1-\alpha}$. Therefore, the Griffiths phase phenomenology leads to a form of the magnetization, susceptibility, and, $C(T)/T$ similar to that found in our experiments.

There has been some discussion in the literature about the ability of magnetic clusters to tunnel into different magnetization states in the presence of itinerant electrons. The presence of the conduction electrons which couple to the local magnetic moments via the Kondo effect cause dissipative effects on the tunneling of magnetic clusters. The dissipation limits the size of clusters allowed to tunnel into opposing magnetization states thus cutting off the singular behavior in the models.[48] Millis *et al.* argue that in heavy fermion metals the electrons are sufficiently well coupled to local magnetic moments, with Kondo temperatures of order 100 K, so that Griffiths phases are unlikely to be observed in these systems.[48] The idea being that the dissipation is relevant at the scale of the Kondo temperature, thus the temperature region where Griffiths phases may be observed is very small. However, Castro Neto and Jones argue that in the region of magnetic clusters the coupling of conduction electrons to the magnetic moments is not important since in these regions the electron density of states is not renormalized by the Kondo effect.[22,23]

In $Fe_{1-x}Co_xS_2$ the relevant energy scales are such that Griffiths phases may be observed over a much wider temperature scale. Here, the Kondo coupling scale is only of order 2 K in the region of the critical Co concentration for ferromagnetism.[12] The Kondo scale is likely so small because the density of electron states, in the approximation of a spherical electron pocket, is proportional to $n_e^{2/3}$ where n_e is the electron density which is more than two orders of magnitude smaller, for the x range investigated here, than in most heavy fermion metals.[12] In addition, the disorder inherent in a doped semiconducting system results in a high scattering rate of the electrons further reducing their ability to screen local moments. Therefore, we expect the dissipation due to a conducting gas of electrons to be a much smaller effect than in the heavy fermion metals where electron densities are much larger and the strong Kondo coupling renormalizes the electron DOS to very high levels. In addition, the relevant energy scale for local moment interactions is commonly estimated by the Curie temperature of the clean magnetic system without dilution. In this case, the clean ferromagnet is CoS_2 and this sets the largest energy scale for local moment interactions at 120 K. Estimates for the average interaction energy of local moments include the Weiss temperature which we have measured via the magnetic susceptibility and is displayed in Fig. 4. From the average and maximum local moment interaction scales compared with the Kondo temperature scale in our materials, we conclude that dissipative effects of the conduction electron gas should be much smaller in $Fe_{1-x}Co_xS_2$ than in heavy fermion metals. However, rounding of the transition due to Kondo coupling of the local moments and the conducting electrons may be relevant at the lowest temperatures.

V. FINITE TEMPERATURE MAGNETIC TRANSITIONS; $x>x_c$

The figures and discussion above give a general description of $Fe_{1-x}Co_xS_2$ as it evolves from a diamagnetic insulator into a ferromagnetic metal. These data establish a magnetic transition that can be observed via the ac magnetic susceptibility down to very low temperatures at very small x. It is clear from our data that magnetic clusters form above T_c and an inhomogeneous magnetic state below T_c. In this section we explore in more detail the behavior of our $Fe_{1-x}Co_xS_2$ crystals having a magnetic phase transition, or perhaps a magnetic glass freezing, at finite temperatures. We examine the frequency and magnetic field dependence of the magnetic

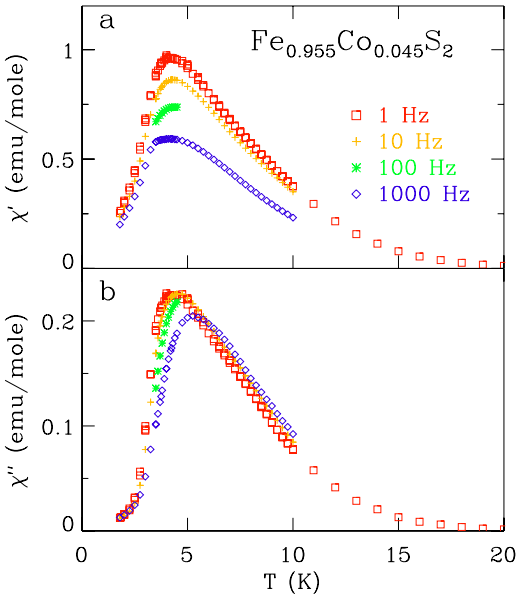

FIG. 21. (Color online) Frequency dependence of the ac susceptibility. The frequency and temperature dependence of the (a) real part, χ', and (b) imaginary part, χ'', of the ac magnetic susceptibility at zero dc field for several $x=0.045$ single crystals. Measurement frequencies were varied between 1 and 1000 Hz as identified in the figure. The excitation field was 1 Oe.

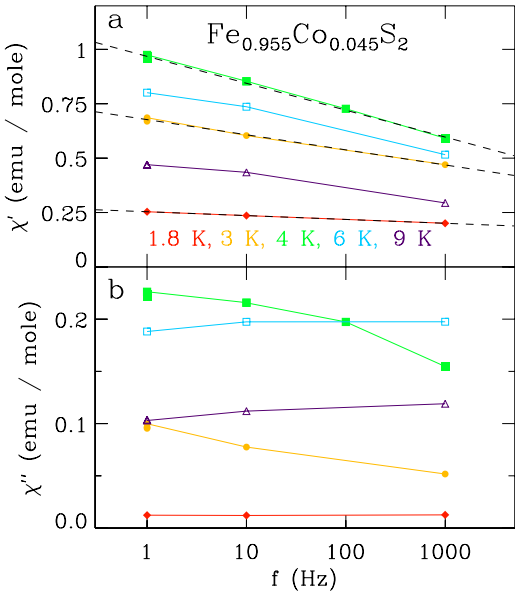

FIG. 22. (Color online) Frequency dependence of the ac susceptibility. The frequency dependence of the real part, χ', (a) and imaginary part, χ'', (b) of the ac magnetic susceptibility at zero dc field for several $x=0.045$ single crystals. Temperatures shown are 1.8 K (red diamonds), 3 K (orange bullets), 4 K (green filled squares), 6 K (blue boxes), and 9 K (violet triangles). The excitation field was 1 Oe. Dashed black lines in frame a are fits to a logarithmic frequency dependence of χ'.

susceptibility both above and below the ordering to compare with typical spin glasses and disordered FMs to gain insight on how such a low density disordered metal establishes a magnetic ground state.

To this end we have carefully measured the f dependence of χ' and χ'' of a few of our samples with $x>x_c$ to probe the low-frequency dynamics of the highly paramagnetic state above T_c as well as the magnetic state below T_c. In Fig. 21 χ' and χ'' of our $x=0.045$ sample is displayed for frequencies between 1 and 1000 Hz. Here, we observe significant decreases in the magnitude of both χ' and χ'', very small changes to the temperature of the maximum in χ' (at most 0.1 K increase) and a larger increase in the temperature of the maximum in χ'' with measurement frequency. We observe no indications of the onset of significant skin effects and eddy current absorption which cause a steady increase in the out-of-phase susceptibility (χ'') with f despite the large out-of-phase component of the signal.

The frequency dependence we measure is similar to the frequency dependent changes that occur in the archetypal spin glass CuMn (Ref. 49) with a relative shift of T_c per decade of measurement frequency of less than 1%. However there are with two important differences with typical spin glass behavior that draw our attention. First, we observe much larger changes in the magnitudes of both χ' and χ'' with frequency than is typical for a metallic spin glass. Second, the temperature range over which we observe a suppression of χ' is from at least $0.5T_c$ to $\sim 2T_c$, whereas for CuMn of similar dopant concentrations there is no measurable f dependence of χ' for reduced temperatures, $(T-T_f)/T_f > 0.05$, where T_f is the spin glass freezing temperature.[49]

The frequency dependence of χ' and χ'' for several temperatures is explicitly demonstrated in Fig. 22 for temperatures near T_c. While χ' decreases monotonically with frequency, χ'' is characterized by a broad peak which moves through the frequency window of our measurement from low f to high f with temperature. At $T<T_c$, $\chi'(f)$ is well described by a logarithmic dependence, as demonstrated in the figure by the dashed lines, with an extrapolated zero crossing between 10^8 and 10^{14} Hz. This dependence has also been observed in insulating spin glasses such as Ising-like $LiHo_xY_{1-x}F_4$.[28] In addition, χ'' has very little f-dependence in the same temperature range so that the dynamic response of the system below T_c is much like that of a spin glass where fluctuations occur on all long time scales.[50] Thus, the magnetic dynamics at these low frequencies resemble that of common spin glass systems, with the added feature that the time dependence extends to temperatures far above T_c.

In addition to the enhanced sensitivity to measurement frequency near T_c our crystals display an enhanced sensitivity to external magnetic fields in the same temperature range. This is demonstrated in Fig. 23 for an $x=0.045$ sample consisting of several small crystals. We note that the data displayed in Fig. 23(a) was previously published[12] and is reproduced here for completeness and comparison of χ' and χ''. In this experiment we have carefully minimized the dc magnetic field for our $H=0$ scan which reveals not only the χ' maximum near 4.5 K but a shoulder ~ 7 K as well. In addition χ'' has two maxima, at 4.5 K and at ~ 7 K. The differences we observe in Fig. 23 with application of very small fields, as well as the appearance of structure in the T sweeps when the field is carefully zeroed are extraordinary. We interpret this sensitivity as an indication of enormous degeneracy, or near degeneracy, of magnetic moment configura-

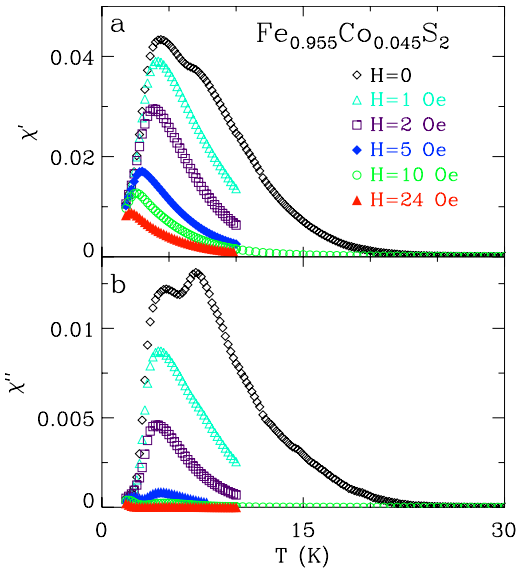

FIG. 23. (Color online) Dramatic field dependence of the ac magnetic susceptibility. The magnetic field, H, and temperature, T dependence of (a) the real part, χ', and (b) imaginary part, χ'', of the ac susceptibility, for the same sample as in Fig. 21 at fields identified in the figure. Data taken with an excitation field of 1 Oe at a frequency of 1 Hz.

tions in these crystals. We observe that dc fields as small as 10 Oe have a significant effect, decreasing the peak value of χ' by a factor of 3.5 and χ'' by more than a factor of 30. The reason for the marked difference between the ac and dc magnetic susceptibilities that we noted above is now quite clear; the dc magnetic susceptibility was measured at fields between 50 and 10^4 Oe applied (dc) field, whereas χ' shows dramatic changes between 0 and 200 Oe in the range $1.8 < T < 20$ K for all samples measured with ac susceptibility techniques at finite H. Therefore, the ac susceptibility data represent a clearer impression of the $H=0$ magnetic state of our $Fe_{1-x}Co_xS_2$ crystals. In addition, the sensitivity to frequency and magnetic fields indicates a complex energy landscape with nearly degenerate energy minima for the magnetic moments. Our main conclusion from the broad temperature and field dependence of M and C in Secs. III A–III C, that clusters of magnetic moments form at $T \gg T_c$, is consistent with the conclusion of a spin glasslike sensitivity to measurement f and applied magnetic fields over a broad T range about T_c.

To aid in understanding the changes that occur to the magnetic response of this system just above the ordering temperature, we have compared $1/\chi'$ taken at small dc magnetic fields as a function of T to the Curie-Weiss form as shown in Fig. 24 for $x=0.023$ and $x=0.045$. What is interesting here is that $1/\chi'$ falls below the Curie-Weiss behavior established at higher temperatures. That is, χ' diverges more strongly than the Curie-Weiss behavior for temperatures substantially above T_c. We note that $1/\chi'$ evolves toward the Curie-Weiss form, $1/\chi' = (T - \Theta_W^{AC})/CC$, with the application of small fields of order 100 Oe for $x=0.023$ and only 10 Oe for $x=0.045$. The strong increase in χ' above T_c and Θ_W is evidence for short ranged ferromagnetic order, or as we have

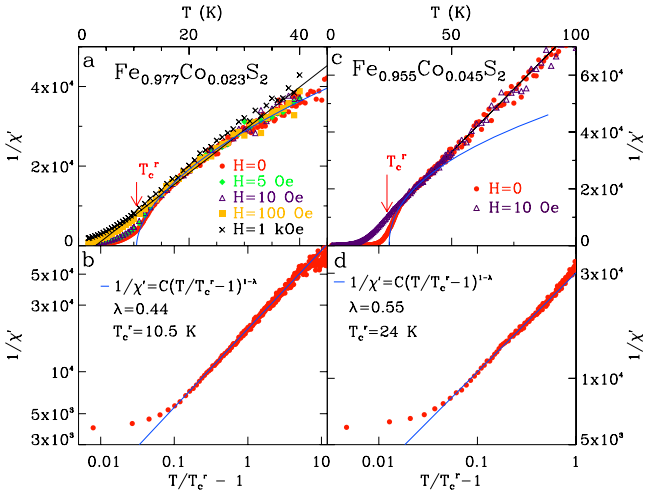

FIG. 24. (Color online) Temperature dependence of the inverse ac magnetic susceptibility. (a) The temperature, T, dependence of the inverse of the real part of the ac magnetic susceptibility, $1/\chi'$ for $x=0.023$, at dc magnetic fields, H, identified in the figure. The black line is the best fit of the Curie-Weiss form to the $H=0$ data between 20 and 50 K with $\Theta_W^{AC}=3.0$ K and a Curie constant corresponding to a population of 1.5×10^{21} cm^{-3} spin 1/2 or 0.061 spin 1/2 per $Fe_{0.977}Co_{0.023}S_2$ formula unit. The blue line is a fit of Eq. (2) in the text to the data with a best-fit value of $\lambda = 0.44 \pm 0.05$ and T_c^r of 10.5 ± 0.5 K identified in the figure by the red arrow. (b) $1/\chi'$ of our $x=0.023$ sample as a function of reduced temperature, $T/T_c^r - 1$, with T_c^r determined from the best fit of Eq. (2) to the data above 11.5 K. The Blue line is the same as in frame a of the figure. (c) T dependence of $1/\chi'$ for $x=0.045$, at H's identified in the figure. The black line is the best fit of the Curie-Weiss form to the $H=0$ data between 25 and 100 K with $\Theta_W^{AC} = 12.8 \pm 0.5$ K and a Curie constant corresponding to a population of 1.8×10^{21} cm^{-3} spin 1/2 or 0.072 spin 1/2 per $Fe_{0.955}Co_{0.045}S_2$ formula unit. The blue line is a fit of Eq. (2) in the text to the data with a best-fit value of $\lambda = 0.55 \pm 0.05$ and T_c^r of 24 ± 0.5 K identified in the figure by the red arrow. (d) $1/\chi'$ of our $x=0.045$ sample as a function of $T/T_c^r - 1$ with T_c^r determined from the best fit of Eq. (2) to the data above 26.5 K. The blue line is the same as in frame c of the figure. Data taken with an excitation field of 1 Oe at a frequency of 1 Hz.

noted above, ferromagnetically aligned clusters of magnetic moment formation.[51] We conclude from this form of χ' that the ground state of this system is likely disordered ferromagnetic rather than a spin-glass state. In the bottom half of Fig. 24 we demonstrate that a power-law temperature-dependent form,[22,24]

$$1/\chi' \propto (T/T_c^r - 1)^{1-\lambda}, \tag{2}$$

with $\lambda \sim 1/2$, describes χ' for 1.5 to 2 orders of magnitude in reduced temperature above T_c^r. Here T_c^r is an indication of the temperature scale where ferromagnetic clusters begin to form and is an indication of the maximum interaction strength between magnetic moments. In contrast, Θ_W^{AC} is an average, or mean-field interaction between magnetic moments. A compilation of λ and T_c^r values from fits of Eq. (2) to $1/\chi'$ for a small number of crystals with x varying between 0.012 and 0.045 is included in Fig. 18. While T_c^r tends to increase

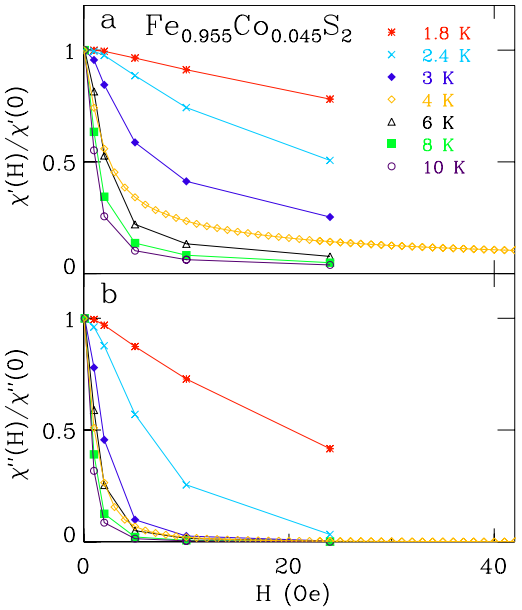

FIG. 25. (Color online) Magnetic-field dependence of the ac magnetic susceptibility. The magnetic field, H, and temperature dependence of (a) the real part, χ', and (b) imaginary part, χ'', of the ac susceptibility, for the same single crystal as in Figs. 21 and 23 at temperatures identified in the figure. Data taken with an excitation field of 1 Oe at a frequency of 1 Hz.

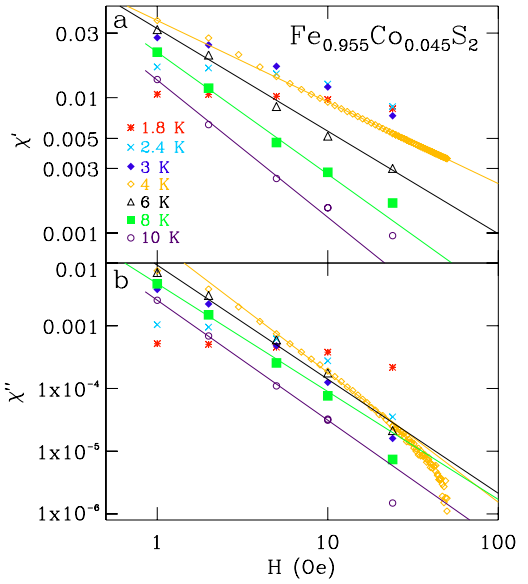

FIG. 26. (Color online) Power-law magnetic field dependence of the ac susceptibility. The magnetic field, H dependence of (a) the real part, χ', and (b) the imaginary part, χ'', of the ac magnetic susceptibility with logarithmic axis for the same $x=0.045$ sample as in Figs. 21, 23, and 25 at temperatures identified in the figure. The lines are power-law fits to the data with best-fit exponents of −0.6 (−2.1) at 4 K, −0.8 (−1.5) at 6 K, −0.9 (−1.7) at 8 K and −1.0 (−1.9) at 10 K for χ' (χ''). Data taken with an excitation field of 1 Oe at a frequency of 1 Hz.

with x, λ takes on values between 0.2 and 0.4 for $x>x_c$.

Beyond the enhanced frequency and magnetic-field dependence seen in Figs. 21 and 23, there are features in our data that indicate that the magnetic state of $Fe_{1-x}Co_xS_2$ is far more interesting than that of a metallic spin glass, particularly for temperatures above T_c. For example, in Fig. 25 we plot the nonlinear ac susceptibility, $\chi'(H)$ and $\chi''(H)$ at temperatures near T_c showing explicitly the changes that occur with H at constant T. Although this figure shows a broad, continuous, decrease in both χ' and χ'' with H for $T<T_c$, it also demonstrates a very sharp low field behavior for $T \geq T_c$. A mean-field analysis of the nonlinear susceptibility involves the assumption of analyticity around $H=0$ such that a power series expansion in even powers, $\chi'(H)=\chi_1+\chi_3H^2+\chi_5H^4+\ldots$ can be employed to describe $\chi'(H)$. The extraordinary field dependence of χ' seen in Fig. 25 cannot be described accurately by this form even over a reduced field range of only 10 Oe for $T>T_c$. Thus the randomness due to the chemical substitutional disorder has modified the field response of this system above T_c such that it is no longer analytic near $H=0$.

This form of $\chi'(H)$ is similar to that found in (body-centered tetragonal) $LiHo_xY_{1-x}F_4$ where the magnetic moments associated with the Ho ions strongly align along the c axis and couple to each other via the dipolar interaction.[52,53] The ground state is ferromagnetic for $x>0.2$ and a spin glass for $0.1<x\leq 0.2$.[52,53] A magnetic field applied transverse to the moments, H_t, causes a mixing of excited states with the ground state doublet. This suppresses the ordering such that a quantum critical point ($T=0$) has been accessed for a large range of x. For $x<0.5$, Refs. 28, 52, and 53 find that $\chi'(H_t \rightarrow 0)$ and $\chi'(H_l \rightarrow 0)$, where H_l is along the c axis, both have a finite slope, $d\chi'/dH$, and thus cannot be expressed in a perturbative expansion in H. The interpretation was that the disorder induced field distribution contains rare large amplitude random fields that prevent a description of $\chi(H_t)$ in a mean-field way as $H\rightarrow 0$. The authors conclude that the nonanalyticity at $H_t=0$ and $T>T_c$ is a manifestation of Griffith singularities.[18] Although there are similarities between our system, $Fe_{1-x}Co_xS_2$ and $LiHo_xY_{1-x}F_4$, both are disordered ferromagnets that are derived by chemical substitution from an insulating parent compound, there are significant differences which are important to point out. The most obvious is that $Fe_{1-x}Co_xS_2$ is a metal for $x\geq 3\times 10^{-4}$, while $LiHo_xY_{1-x}F_4$ remains insulating for all x. In addition, $LiHo_xY_{1-x}F_4$ is strongly Ising-like with the magnetic moments preferring to align along the c axis. In contrast, $Fe_{1-x}Co_xS_2$ is cubic and for $x=1$ has been shown to have a very small cubic anisotropy of its magnetization so that it been described as Heisenberg-like.[54] However, we find that both of these disordered magnets contain rare large amplitude fluctuations that are the hallmarks of Griffiths phase formation for $T>T_c$. Thus, not only do we find evidence for such phases in samples on the verge of magnetic ordering at $T=0$, but also discover evidence for similar rare region effects at larger x, $x>x_c$ above the ordering temperature.

In contrast to mean-field forms, the magnetic field dependence of χ' shown in Fig. 25 can instead be well described as a simple power law in H at $T>T_c$ as demonstrated in Figs. 26 and 27. These figures demonstrate that a small power-law form, $\chi'=\chi_0H^{\alpha_M-1}$, with α_M between 0 and 1 describes the data over at least a decade and 1/2 in field for

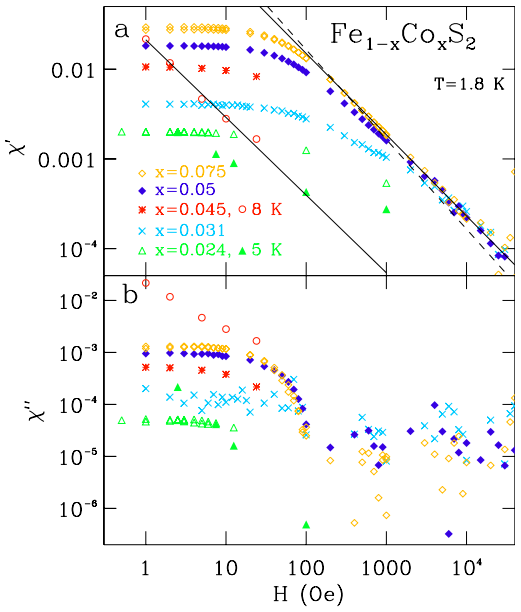

FIG. 27. (Color online) Magnetic field dependence of the ac susceptibility for various Co densities larger than critical concentration. The magnetic field, H dependence of (a) the real part, χ', and (b) the imaginary part, χ'', of the ac magnetic susceptibility at 1.8 K with logarithmic axis for $Fe_{1-x}Co_xS_2$ for x's identified in the figure. Data at one $T>T_c$ are shown for the $x=0.024$ (5 K) and $x=0.045$ (8 K) crystals to demonstrate the changes that occur to the low field behavior. The solid lines are power-law fits to the data with best-fit power law of −0.9 for the high field data at $T=1.8$ K as well as for the data for $x=0.045$ at 8 K. Dashed line is a H^{-1} dependence for comparison. Data taken with an excitation field of 1 Oe at a frequency of 1 Hz.

$T>T_c$, while for $T<T_c$ a much more gentle field dependence is seen. The best-fit α_M values have been included in Fig. 18 for two samples where we have sufficient data for an accurate determination of this parameter. In addition, χ'' can also be described in a power-law form with an exponent between −1.3 and −2.0. For fields between 50 and 100 Oe χ'' is seen to undergo a much steeper decrease so that above these fields it is consistent with zero being no larger than the backgrounds in our measurement. The small power-law form for $\chi'(H)$ at $T>T_c$ is consistent with the Griffiths phase hypothesis made on the basis of the temperature dependence above.

Figure 27 displays χ' and χ'' at 1.8 K for 5 different samples with $x>x_c$ and demonstrates several features that are common. First we note that for these Co concentrations $T_c>1.8$ K and, as discussed above, χ' is not strongly field dependent below about 100 Oe at this temperature. This is in contrast to the data shown above T_c, a small subset of which is shown in the figure for comparison. For larger fields, χ' is seen to decrease as $H^{-0.9\pm0.1}$ while χ'' is suppressed to within the background level of zero above this same field scale. It is interesting to note that χ' above 10^3 Oe is less dependent on x suggesting that here the magnetic energy level distribution is much more independent of x.

Our presentation in this section has focused on the ac magnetic susceptibility of our $Fe_{1-x}Co_xS_2$ crystals with $x>x_c$ which demonstrates that we have discovered several unusual aspects. This includes a highly frequency dependent χ' and χ'' which encompasses a temperature range both above and below T_c that is much larger than in prototypical spin glass systems. We have found an extraordinary nonanalytic field dependence to the ac susceptibility near $H=0$ coupled with a small power-law form to the temperature dependence. These aspects are indicative of an inhomogeneous magnetic system where rare ordered regions form at temperatures above the long-range ordering, or perhaps a glass-like freezing, temperature of the disordered system. These local ferromagnetically ordered regions are well described by the Griffiths phase phenomenology[18–20,22] where the nonuniversal power-law dependent properties are the result of quantum mechanical tunneling of these rare regions to states with different magnetizations.

VI. DISCUSSION AND CONCLUSIONS

In this paper, we have described a set of experiments exploring the nucleation of a magnetic ground state in a carrier-doped nonmagnetic insulator. For this investigation we chose the relatively simple diamagnetic insulator FeS_2 as it allows for Co substitution for Fe without the formation of second phases.[13–17] In addition, the end member of the series CoS_2 is an itinerant ferromagnet with a Curie temperature of 120 K.[14] We found that the Co substitution yields a small number of itinerant charge carriers[29] and magnetic moments that are likely localized to the Co impurity sites. A weakly coupled magnetic ground state, spin glass, or disordered ferromagnetic, developed for $x\geq0.007\pm0.002$ as evidenced by a peak in the temperature dependence of the magnetic susceptibility. As x is increased beyond x_c the magnetic state becomes more robust to temperature and magnetic field so that the FM state is more evident at fields and temperatures where common tests can easily be performed.

In the paramagnetic regions of temperature and Co concentration, we found fluctuating magnetic moments whose size was significantly larger than that expected for spin-1/2 moments of individual Co dopants in an FeS_2 background. This led us to the conclusion that clusters of magnetic moments were forming upon cooling below 10 K for samples with $x<x_c$ and at $T>T_c$ for sample with $x>x_c$. The formation of clusters of average size of 3 to $5J=1/2$ magnetic moments was also found to be consistent with the measured $C(T)/T$ and the entropy derived from it. Because of the disorder and assumed random placement of Co impurities throughout our samples, it is likely that a distribution of cluster sizes results. This distribution is likely to have a very long tail for large cluster sizes so that there may be rare regions of local magnetic order. Such a description fits in well with the sensitivity to magnetic fields that we observed in the susceptibility and magnetization of our crystals.

We posit that it is these rare regions of incipient order that cause the unusual temperature and magnetic field dependencies that we measured in the magnetic susceptibility and specific heat. The consistent appearance of small power laws in our analysis of both the low-temperature behavior of samples in proximity to x_c, and at temperatures just above T_c for samples with $x>x_c$, lead us to conclude that Griffiths phase

physics is the most likely mechanism determining the static and dynamic properties of this system.[19,20] In this scenario large rare regions of order appear in disordered magnets at temperatures below the critical temperature of the system without disorder. These ordered regions which act as single large magnetic moments are subject to tunneling events where the magnetic moment reverses. When a distribution of cluster sizes is included, small power-law temperature dependences are predicted. Details such as the anisotropies (Ising-like or Heisenberg-like moments) as well as the mechanisms for dissipation are thought to determine the observability conditions for these effects.[19,20] $Fe_{1-x}Co_xS_2$ appears to be a system where such effects may be observable over a wide temperature range as the Kondo temperatures we measure are small, of order 1 K,[12] while the Weiss temperatures are typically much larger, so that dissipation by way of the charge carriers may be relevant only at the lowest temperatures.

It is no surprise that the disorder inherent to a doped semiconducting system can lead to the formation of an inhomogeneous magnetic state at low temperatures. What we find extraordinary are the unusual power-law temperature and magnetic-field dependencies of physical properties that we measure along with the very sharp, nonanalytic, field dependence of the magnetic susceptibility near $H=0$. That a simple model of disordered magnets[18] which postulates the existence of rare ordered regions can describe the broad features of such a complicated system is both surprising and compelling.

ACKNOWLEDGMENTS

We thank I. Vekhter and C. Capan for discussions. J.F.D., D.P.Y., and J.Y.C. acknowledge support of the NSF under Grants No. DMR084376, No. DMR0449022, and No. DMR0756281. We thank J. M. Honig for providing crystals of $V_{0.99}Ti_{0.01}O_3$ for use as a manometer in our pressure cells.

[1] S. A. Wolf, D. D. Awschalom, R. A. Buhrman, J. M. Daughton, S. von Molnar, M. L. Roukes, A. Y. Chtchelkanova, and D. M. Treger, Science **294**, 1488 (2001).
[2] S. Von Molnar and D. Read, Proc. IEEE **91**, 715 (2003).
[3] H. Ohno, A. Shen, F. Matsukura, A. Oiwa, A. Endo, S. Katsumotos, and Y. Iye, Appl. Phys. Lett. **69**, 363 (1996).
[4] H. Ohno, H. Munekata, T. Penney, S. von Molnar, and L. L. Chang, Phys. Rev. Lett. **68**, 2664 (1992).
[5] F. Matsukura, H. Ohno, A. Shen, and Y. Sugawara, Phys. Rev. B **57**, R2037 (1998).
[6] M. L. Reed, N. A. El-Masry, H. H. Stadelmaier, M. K. Ritums, M. J. Reed, C. A. Parker, J. C. Roberts, and S. M. Bedair, Appl. Phys. Lett. **79**, 3473 (2001).
[7] R. C. Myers, B. L. Sheu, A. W. Jackson, A. C. Gossard, P. Schiffer, N. Samarth, and D. D. Awschalom, Phys. Rev. B **74**, 155203 (2006).
[8] G. Salis, Y. Kato, K. Ensslin, D. C. Driscoll, A. C. Gossard, and D. D. Awschalom, Nature (London) **414**, 619 (2001).
[9] D. J. Priour and S. Das Sarma, Phys. Rev. Lett. **97**, 127201 (2006).
[10] V. M. Galitski, A. Kaminski, and S. Das Sarma, Phys. Rev. Lett. **92**, 177203 (2004).
[11] T. C. Schulthess, W. M. Temmerman, Z. Szotek, W. H. Butler, and G. M. Stocks, Nature Mater. **4**, 838 (2005).
[12] S. Guo, D. P. Young, R. T. Macaluso, D. A. Browne, N. L. Henderson, J. Y. Chan, L. L. Henry, and J. F. DiTusa, Phys. Rev. Lett. **100**, 017209 (2008).
[13] H. S. Jarrett, W. H. Cloud, R. J. Bouchard, S. R. Butler, C. G. Fredric, and J. L. Gillson, Phys. Rev. Lett. **21**, 617 (1968).
[14] R. J. Bouchard, Mater. Res. Bull. **3**, 563 (1968).
[15] K. Ramesha, R. Seshadri, C. Ederer, T. He, and M. A. Subramanian, Phys. Rev. B **70**, 214409 (2004).
[16] L. Wang, T. Y. Chen, C. L. Chien, J. G. Checkelsky, J. C. Eckert, E. D. Dahlberg, K. Umemoto, R. M. Wentzcovitch, and C. Leighton, Phys. Rev. B **73**, 144402 (2006).
[17] S. F. Cheng, G. T. Woods, K. Bussmann, I. I. Mazin, R. J. Soulen, E. E. Carpenter, B. N. Das, and P. Lubitz, J. Appl. Phys. **93**, 6847 (2003).
[18] R. B. Griffiths, Phys. Rev. Lett. **23**, 17 (1969).
[19] E. Miranda and V. Dobrosavljevic, Rep. Prog. Phys. **68**, 2337 (2005).
[20] T. Vojta, J. Phys. A **39**, R143 (2006).
[21] G. R. Stewart, Rev. Mod. Phys. **73**, 797 (2001).
[22] A. H. Castro Neto, G. Castilla, and B. A. Jones, Phys. Rev. Lett. **81**, 3531 (1998).
[23] A. H. Castro Neto and B. A. Jones, Phys. Rev. B **62**, 14975 (2000).
[24] M. B. Salamon, P. Lin, and S. H. Chun, Phys. Rev. Lett. **88**, 197203 (2002).
[25] J. Deisenhofer *et al.*, Phys. Rev. Lett. **95**, 257202 (2005).
[26] Y. Shimada, S. Miyasaka, R. Kumai, and Y. Tokura, Phys. Rev. B **73**, 134424 (2006).
[27] J. Herrero-Albillos, L. M. Garcia, and F. Bartolome, J. Phys.: Condens. Matter **21**, 216004 (2009).
[28] C. Ancona-Torres, D. M. Silevitch, G. Aeppli, and T. F. Rosenbaum, Phys. Rev. Lett. **101**, 057201 (2008).
[29] S. Guo, D. P. Young, R. T. Macaluso, D. A. Browne, N. L. Henderson, J. Y. Chan, L. L. Henry, and J. F. DiTusa, following paper, Phys. Rev. B **81**, 144424 (2010).
[30] L. Neél and R. Benoit, C. R. Hebd. Seances Acad. Sci. **237**, 444 (1953).
[31] I. I. Mazin, Appl. Phys. Lett. **77**, 3000 (2000).
[32] S. Guo, Ph. D thesis, Louisiana State University, 2006.
[33] K. Murata, H. Yoshino, H. O. Yadav, Y. Honda, and N. Shirakawa, Rev. Sci. Instrum. **68**, 2490 (1997).
[34] K. Koyama, S. Hane, K. Kamishima, and T. Goto, Rev. Sci. Instrum. **69**, 3009 (1998).
[35] K. Kamishima, M. Hagiwara, and H. Yoshida, Rev. Sci. Instrum. **72**, 1472 (2001).
[36] S. A. Carter, T. F. Rosenbaum, M. Lu, H. M. Jaeger, P. Metcalf, J. M. Honig, and J. Spalek, Phys. Rev. B **49**, 7898 (1994).
[37] R. G. Goodrich, D. Hall, E. Palm, and T. Murphy, Cryogenics

38, 221 (1998).
[38] A. Arrott and J. E. Noakes, Phys. Rev. Lett. **19**, 786 (1967).
[39] M. B. Maple, J. Wittig, and K. S. Kim, Phys. Rev. Lett. **23**, 1375 (1969).
[40] J. F. DiTusa, K. Friemelt, E. Bucher, G. Aeppli, and A. P. Ramirez, Phys. Rev. Lett. **78**, 2831 (1997).
[41] Y. Nishino, M. Kato, S. Asano, K. Soda, M. Hayasaki, and U. Mizutani, Phys. Rev. Lett. **79**, 1909 (1997).
[42] M. Lakner, H. v. Lohneysen, A. Langenfeld, and P. Wolfle, Phys. Rev. B **50**, 17064 (1994).
[43] R. N. Bhatt and P. A. Lee, Phys. Rev. Lett. **48**, 344 (1982).
[44] M. A. Paalanen, J. E. Graebner, R. N. Bhatt, and S. Sachdev, Phys. Rev. Lett. **61**, 597 (1988).
[45] See, e.g., S. Blundell, *Magnetism in Condensed Matter* (Oxford University Press, Oxford, 2001).
[46] T. Westerkamp, M. Deppe, R. Kuchler, M. Brando, C. Geibel, P. Gegenwart, A. P. Pikul, and F. Steglich, Phys. Rev. Lett. **102**, 206404 (2009).
[47] See e.g., N. W. Ashcroft and N. D. Mermin, *Solid State Physics* (Saunders College, Philadelphia, 1976).
[48] A. J. Millis, D. K. Morr, and J. Schmalian, Phys. Rev. B **66**, 174433 (2002).
[49] C. A. M. Mulder, A. J. van Duyneveldt, and J. A. Mydosh, Phys. Rev. B **23**, 1384 (1981).
[50] K. Binder and A. P. Young, Rev. Mod. Phys. **58**, 801 (1986).
[51] See, e.g., Z. W. Ouyang, V. K. Pecharsky, K. A. Gschneidner, D. L. Schlagel, and T. A. Lograsso, Phys. Rev. B **74**, 094404 (2006).
[52] Wenhao Wu, B. Ellman, T. F. Rosenbaum, G. Aeppli, and D. H. Reich, Phys. Rev. Lett. **67**, 2076 (1991).
[53] D. M. Silevitch, D. Bitko, J. Brooke, S. Ghosh, G. Aeppli, and T. F. Rosenbaum, Nature (London) **448**, 567 (2007).
[54] H. Hiraka and Y. Endoh, J. Phys. Soc. Jpn. **63**, 4573 (1994).